Supporting Information

In-situ Constructing Hydrophobic Channel Interconnecting Progressively Zincophilic Planes for Stable Zn Metal Anode

Miao Yu, Jiawei Mu, Lingfeng Wang, Yuchao Niu, Wenjie Si, Jiale Li, Xiaoyu Liu, Tiantian Li, Xiangcun Li, Wenji Zheng, Yan Dai, Xiaobin Jiang, Gaohong He**

Experimental Section

Preparation of electrolytes: 2 M $ZnSO_4$ (ZS) electrolyte was prepared by dissolving zinc sulfate heptahydrate ($ZnSO_4 \cdot 7H_2O$, 99.995% Aladdin) into the deionized water. Certain amounts of sulfobutylether-β-cyclodextrin (SCD, 99%, Macklin) were further added into the ZS electrolyte to prepare ZS + *x* mM SCD, where *x* = 5/10/15/20. Unless otherwise specified, ZS + SCD refers to ZS + 10 mM SCD.

Synthesis of $NH_4V_4O_{10}$: 1.17 g NH_4VO_3 and 1.89 g $C_2H_2O_4 \cdot H_2O$ were dissolved in 70 mL deionized water. Then, transferring the solution into the reactor and heating to the 140 °C for 48 h. Afterward, washing the product several times with deionized water and ethanol, then drying it at 60 °C for 12 h to gain the material of the $NH_4V_4O_{10}$.

Preparation of $NH_4V_4O_{10}$ cathode: $NH_4V_4O_{10}$, super-P and PVDF were mixed at a mass ratio of 7:2:1 in N-methyl pyrrolidone (NMP). Then, coated on both sides of carbon paper and dried at 60 °C for 12 h. In final, cutting it into 12 mm disc. The mass loading of active materials was between 2 - 2.5 mg cm^{-2}.

Fabrications of Zn//Cu asymmetric cells, Zn//Zn symmetric cells and Zn//$NH_4V_4O_{10}$ full cells: Zn//Cu asymmetric cells were assembled in CR2032 coins using Zn plates as the anode, Cu plates as the cathode, Whatman GF/A membranes as the separator, and ZS or ZS + *x* mM SCD as electrolytes. Cu plates were replaced by Zn plates in Zn//Zn symmetric cells, and $NH_4V_4O_{10}$ cathode discs in Zn//$NH_4V_4O_{10}$ full cells. Zn//$NH_4V_4O_{10}$ pouch cell (4 cm * 4.5 cm) was assembled using the same cathode, separator, 30 μm Zn foil, and ~ 1 mL ZS + SCD electrolyte, which were sealed in the aluminum laminated film with nickel tabs.

Materials characterizations: The structure and morphology of the anodes and cathodes were characterized by field emission scanning electron microscopy (FE-SEM, JEOL JSM 7610F Plus) and X-ray diffraction (XRD, Bruker D8 Advance). Fourier transformed infrared spectroscopy (FT-IR, Thermo Fisher Scientific Nicolet iS20), Raman spectroscopy (Horiba LabRAM HR Evolution), nuclear magnetic resonance (NMR, Bruker AVANCE III 500) were applied to investigate the properties of electrolytes. X-ray photoelectron spectroscopy (XPS, ESCALAB Xi+) was applied to investigate the interaction between SCD and Zn. The pH value, viscosity and ionic conductivity of the electrolytes were measured with corresponding meters. *In-situ* optical microscopy (Yuescope, YM710TR) was used to observe the Zn plating process, and confocal laser optical microscopy (CLMS, ZYGO Corporation, NewView9000) was used to characterize the surface roughness of the electrodes.

Electrochemical measurements: Linear sweep voltammetry (LSV), Tafel plots, cyclic voltammetry (CV) curves, chronoamperometry (CA) curves, and electrochemical impedance spectroscopy (EIS) were collected using electrochemical workstations (PARSTAT MC and Shanghai Chenhua CHI760e). LSV and Tafel plots were characterized using a three-electrode system, with Pt mesh as the counter electrode, Ag/AgCl electrode and the reference electrode and Zn plate as the working electrode, respectively. LSV curves were collected from -1 to -2.5 V with a scan rate of 2 mV s^{-1} using 1 M Na_2SO_4 and 1 M Na_2SO_4 + 10 mM SCD as electrolytes. Tafel plots were collected from -0.6 to -1.5 V with a scan rate of 5 mV s^{-1} using 2 M $ZnSO_4$ and 2 M $ZnSO_4$ + 10 mM SCD as electrolytes. Zn^{2+} transference number was calculated according to $t_{Zn^{2+}} = I_s(\Delta V - I_oR_o)/I_o(\Delta V - I_sR_s)$, where ΔV is the applied voltage of the polarization tests (20 mV), I_0 and R_0 are the initial current and resistance, and I_s and R_s are the steady-state current and resistance, respectively. Galvanostatic charge/discharge (GCD) curves, coulombic efficiency (CE) and battery performance were tested using a LAND CT3002A multichannel battery test system.

Theoretical calculations: The DFT calculations were employed the Vienna Ab initio Simulation Package (VASP) within the generalized gradient approximation (GCA) using the Perdew-Burke-Ernzerhof (PBE) and chosen the projected augmented wave (PAW) potentials to describe the ionic cores and take valance electrons into account using a plane wave basis set with a kinetic energy cutoff of 450 eV. Partial occupancies of the Kohn−Sham orbitals were allowed using the Gaussian smearing method and a width of 0.05 eV.[1-5] For the optimization of both geometry and lattice size, the Brillouin zone integration was performed with a 1 x 1 x 1 k-mesh Monkhorst-Pack sampling.[6] The self-consistent calculations applied a convergence energy threshold of 10^{-5} eV. The equilibrium geometries and lattice constants were optimized with maximum stress on each atom within 0.02 eV $Å^{-1}$. The 15 Å vacuum layer was normally added to the surface to eliminate the artificial interactions between periodic images. The weak interaction was described by DFT+D3 method using empirical correction in Grimme's scheme.[7-8] Spin polarization method was adopted to describe the magnetic system. The adsorption energy was calculated as: $E_{ads} = E_{(*adsorbent)} - E_{(*)} - E_{(adsorbent)}$. $E_{(*adsorbent)}$, $E_{(*)}$ and $E_{(adsorbent)}$ represent the total energy of *adsorbent, * and adsorbent molecule, respectively. The quantum chemistry calculations were carried out with the Gaussian 16 software. The B3LYP hybrid functional[9] was applied for all calculations in combination with the D3BJ dispersion correction.[8] For geometry optimization, the mixed basis set (BS1) of SDD for Zn element and 6-31G(d,p) for other atoms with the IEFPCM solvent model[10] for water were used. The geometries were fully optimized without any structural

constraints. The final and solvation energies for the fully optimized structures in the water were calculated by employing the SMD continuum solvation model[11] with the larger mixed basis set (BS2) of SDD for Zn and 6-311G(d,p) for other atoms. The molecular orbitals figures and electrostatic potential surfaces were extracted from the Multiwfn 3.8 program[12] and visualized using the visual molecular dynamics (VMD)[13] software. The binding energy (E_b) was calculated by the following equation: $E_b = E_{Complex} - (E_{M1} + E_{M2})$, where $E_{Complex}$, E_{M1}, and E_{M2} represent the energies of the complex, and energies of the interacting molecules, respectively.

Molecular dynamics simulation: All molecular dynamics (MD) simulation were performed using the Gromacs 2021 package.[14] The simulation box size of 10×10×10 nm^3 was used in all simulations. There were two simulation systems, in which included 1200 Zn^{2+}, 1200 SO_4^{2-}, H_2O with/without 6 SCD. The zinc plate was slightly positively charged to simulate the experimental situation. The crystal model of Zn (110) was obtained from Materials Studio and then cleaved. The force field parameters used for Zn plate were derived from the Universal force field and the Zn^{2+}, SO_4^{2-} and SCD were assigned with OPLS-AA force field parameters. The models for exploring the adsorption configuration of SCD on zinc plates included one zinc plate and six SCD molecules randomly placed above the zinc plates. Under the LINCS algorithm, all the bonds with H atoms were constrained. Each system was simulated ensemble for 100 ns under the NPT. The experimental temperature was set as 298 K, and under Berendsen, the pressure was set as 1 bar. The cut-off for the long-range electrostatic interaction was set as 1.0 nm, the same as the cut-off for the nonbonded van der Waals interaction. The time step is 1 fs in each system. The binding process, molecular surface diagrams of the final binding area and the binding energy of different residues on the material surface were analyzed for each system.

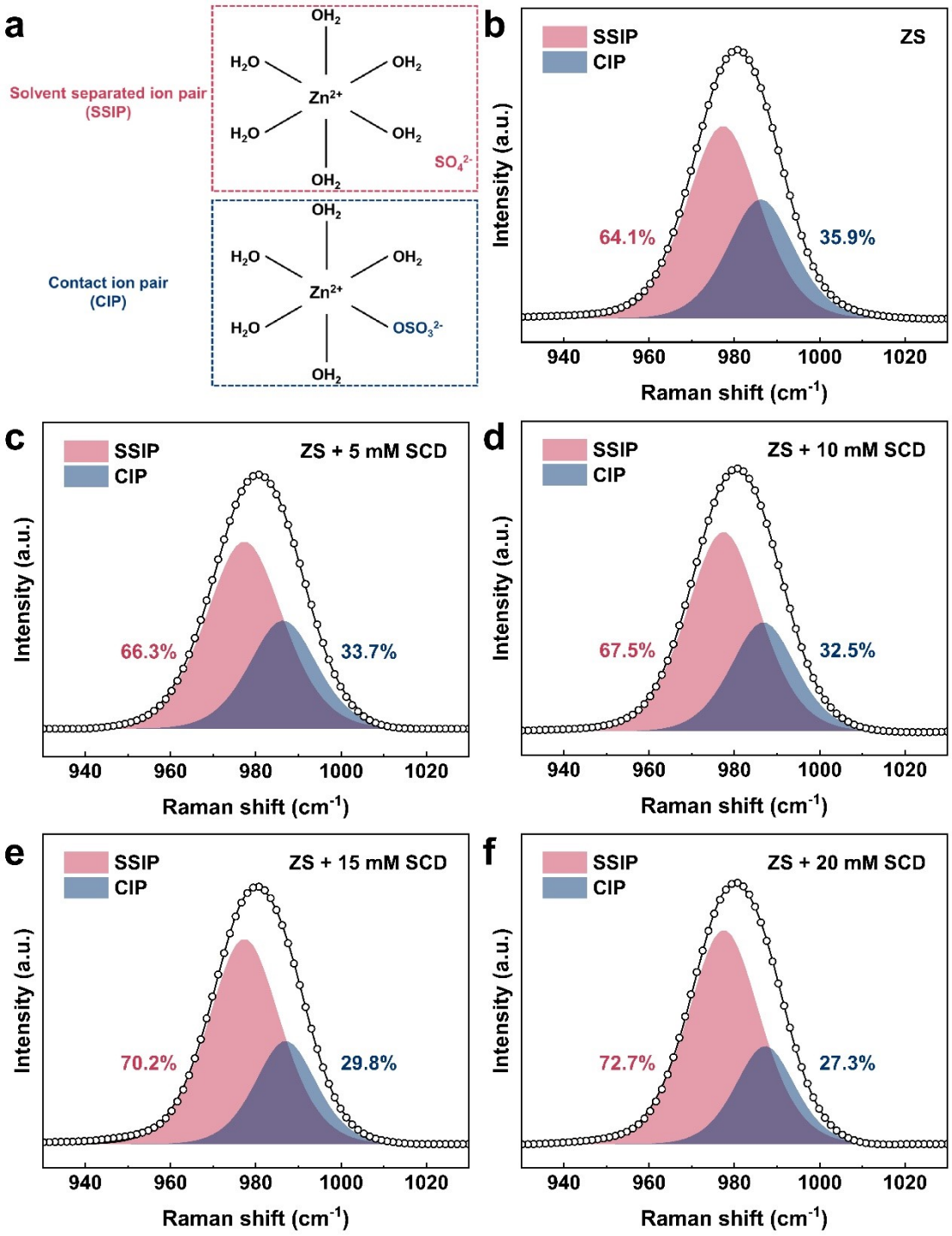

Figure S1. a) The illustration of solvent separated ion pair (SSIP) and contact ion pair (CIP), and b-f) the detailed contribution of SSIP and CIP in the Raman spectra of different electrolytes.

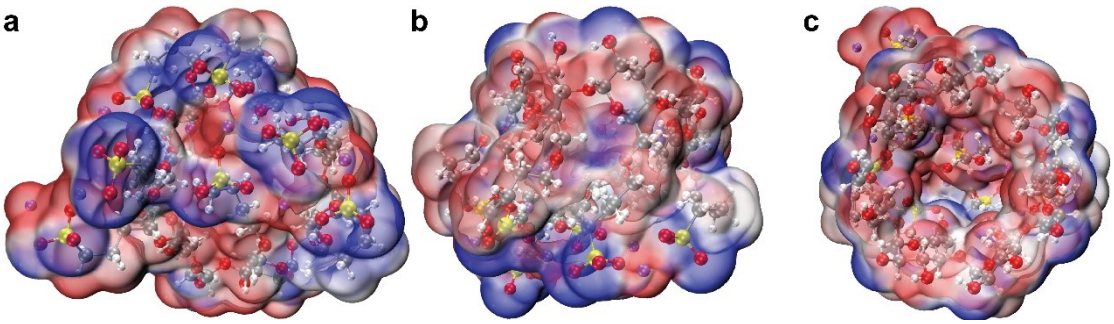

Figure S2. Different views of the ESP of SCD molecule.

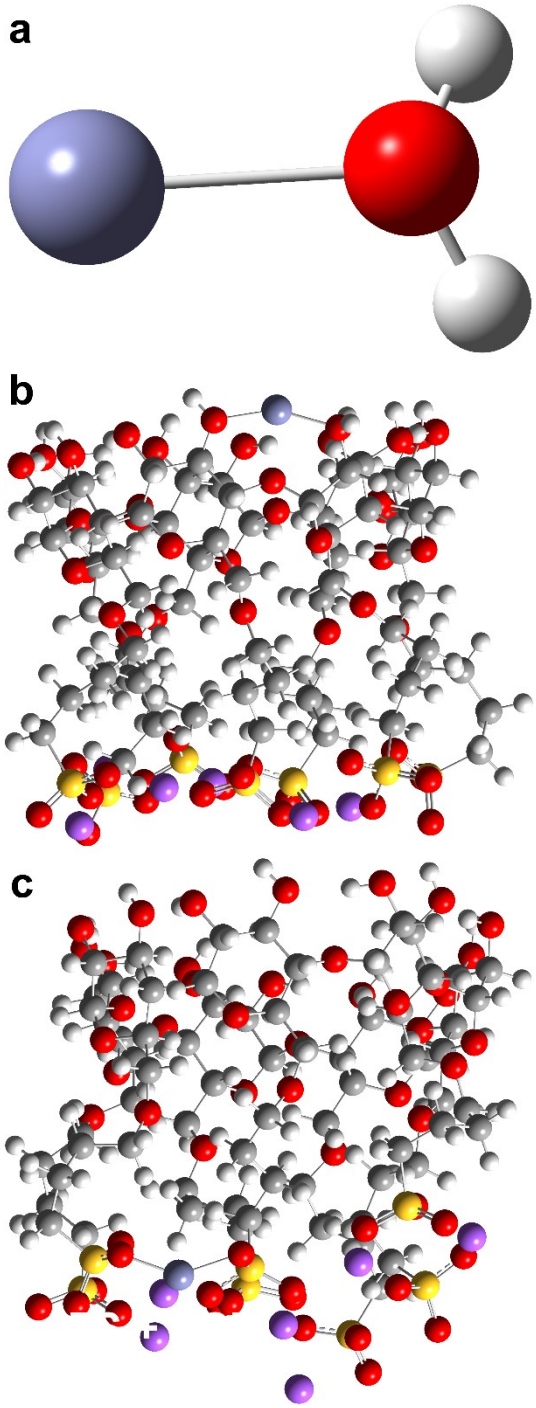

Figure S3. The enlarged binding configurations of Zn^{2+} with a) H_2O, and b) the OH group and c) SO_3^- group in SCD.

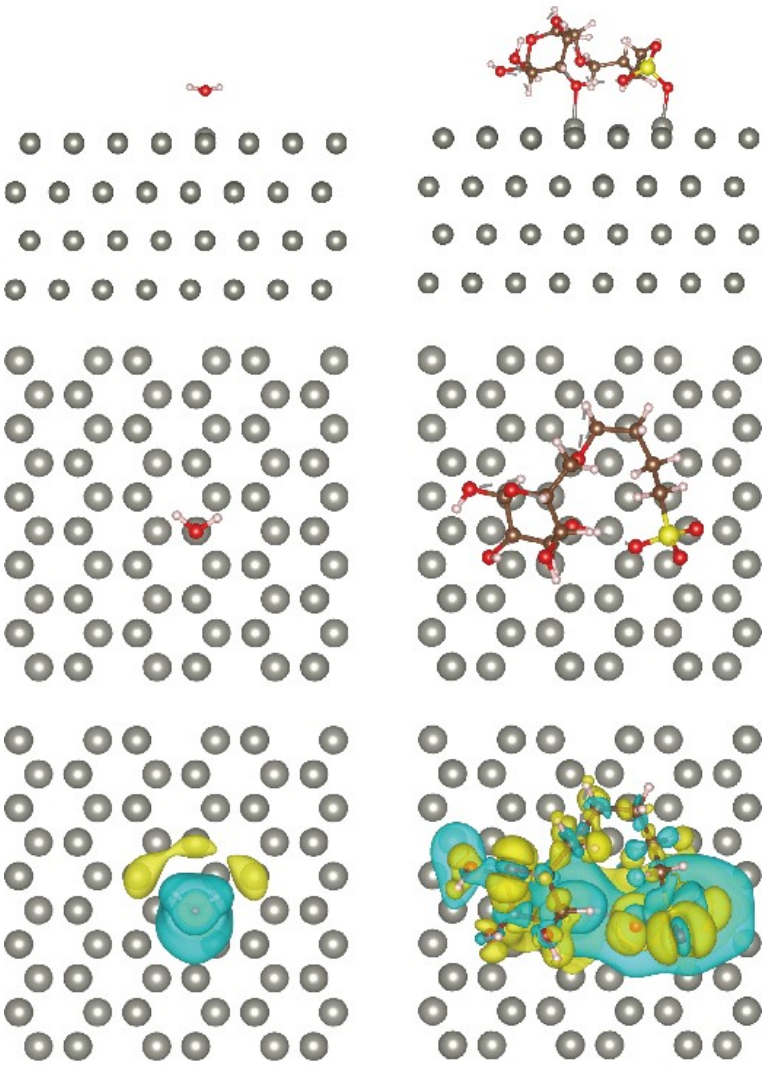

Figure S4. Different views of the adsorption configurations and differential charge densities of H_2O and SCD unit on Zn surface.

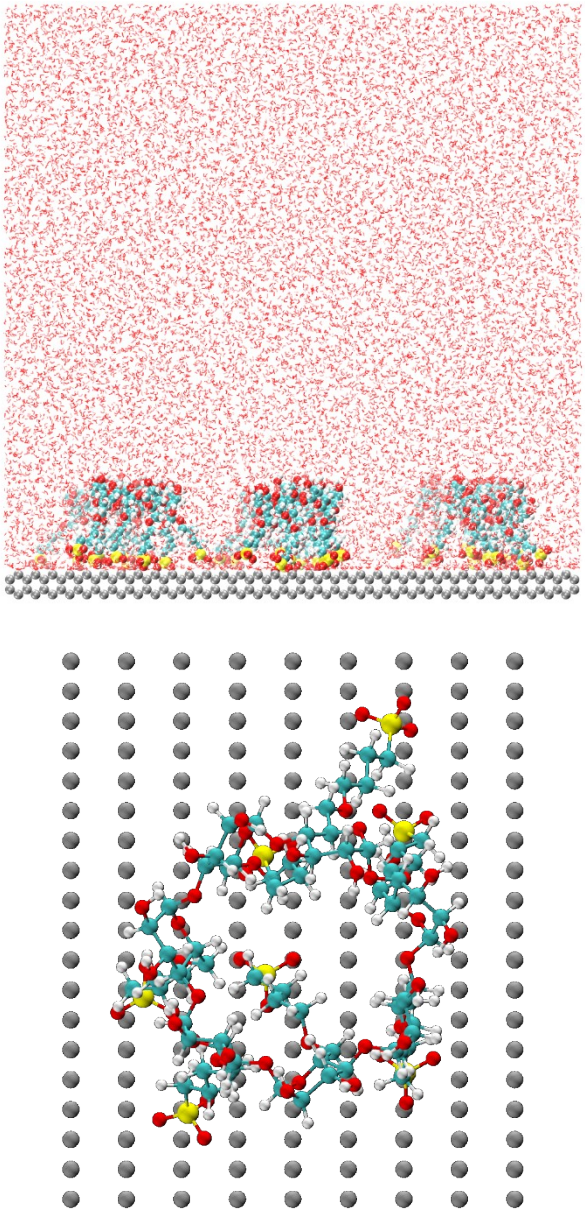

Figure S5. 3D snapshot of the MD simulated adsorption of SCD on Zn surface, and the top view of the enlarged adsorption configuration.

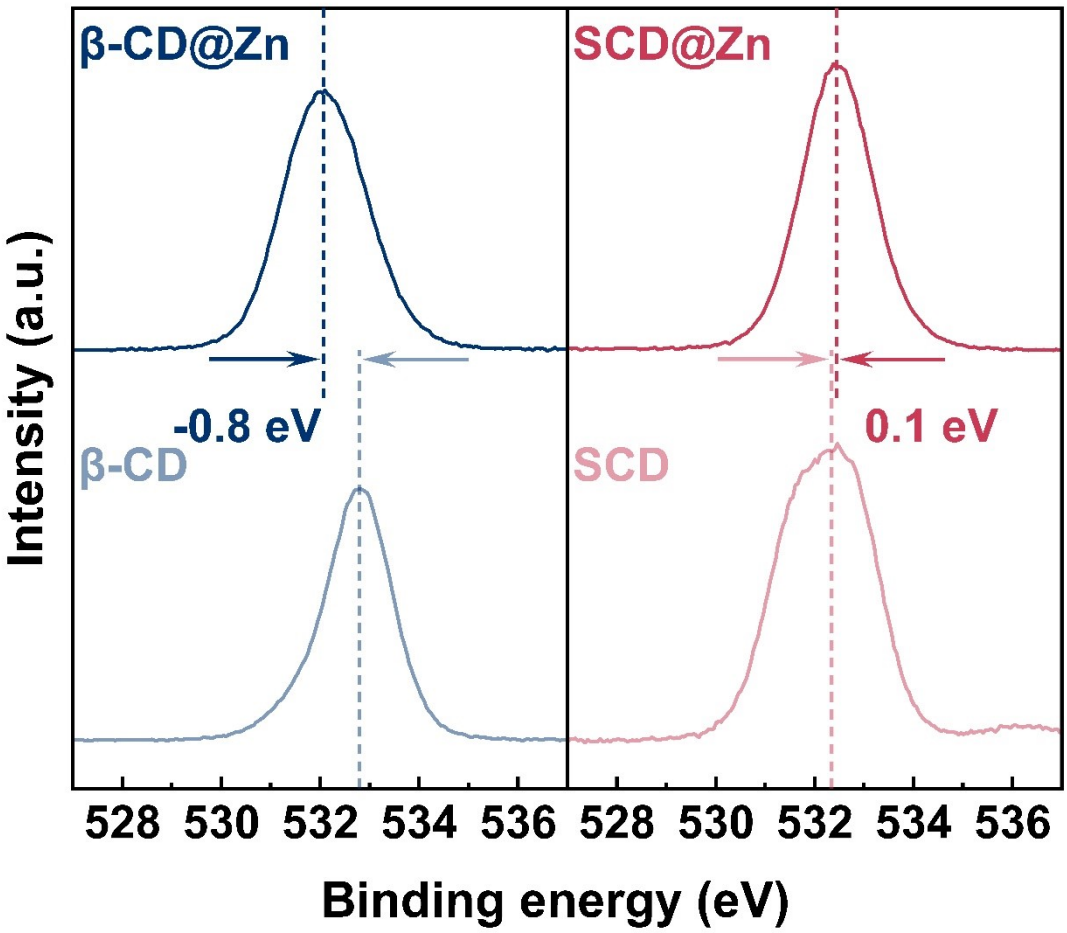

Figure S6. The XP spectra of O 1s of the β-CD and SCD adsorbed Zn surface, and corresponding powders.

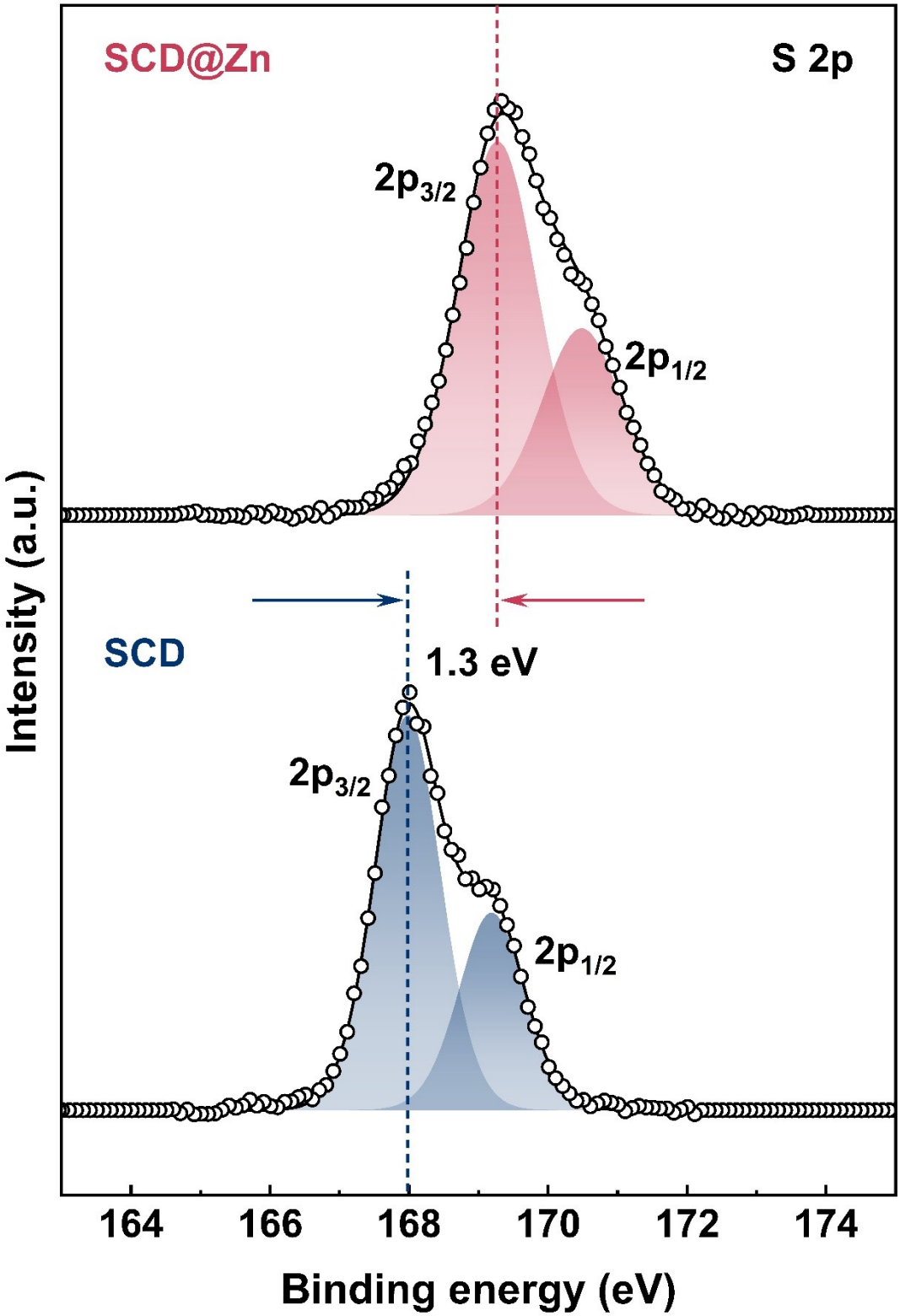

Figure S7. The XP spectra of S 2p of the SCD adsorbed Zn surface, and corresponding powders.

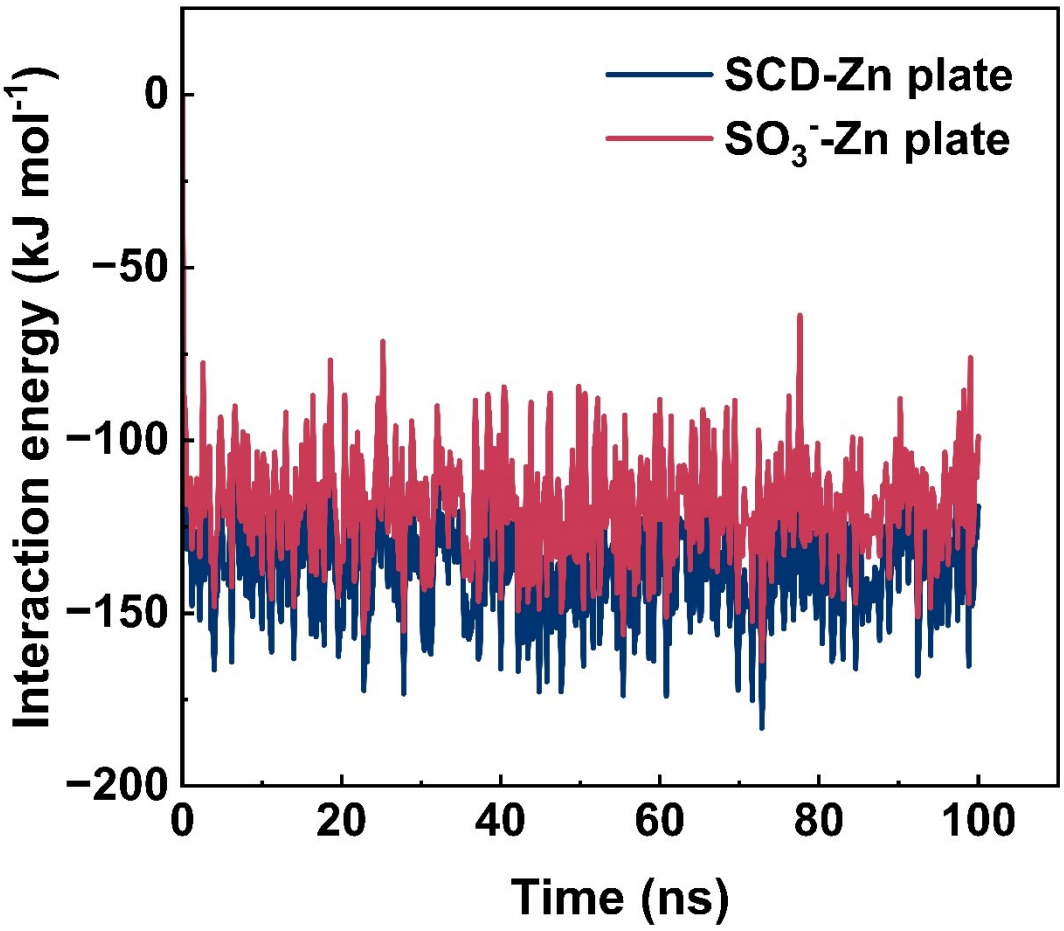

Figure S8. Relative interaction energy of SCD molecules and SO_3^- groups.

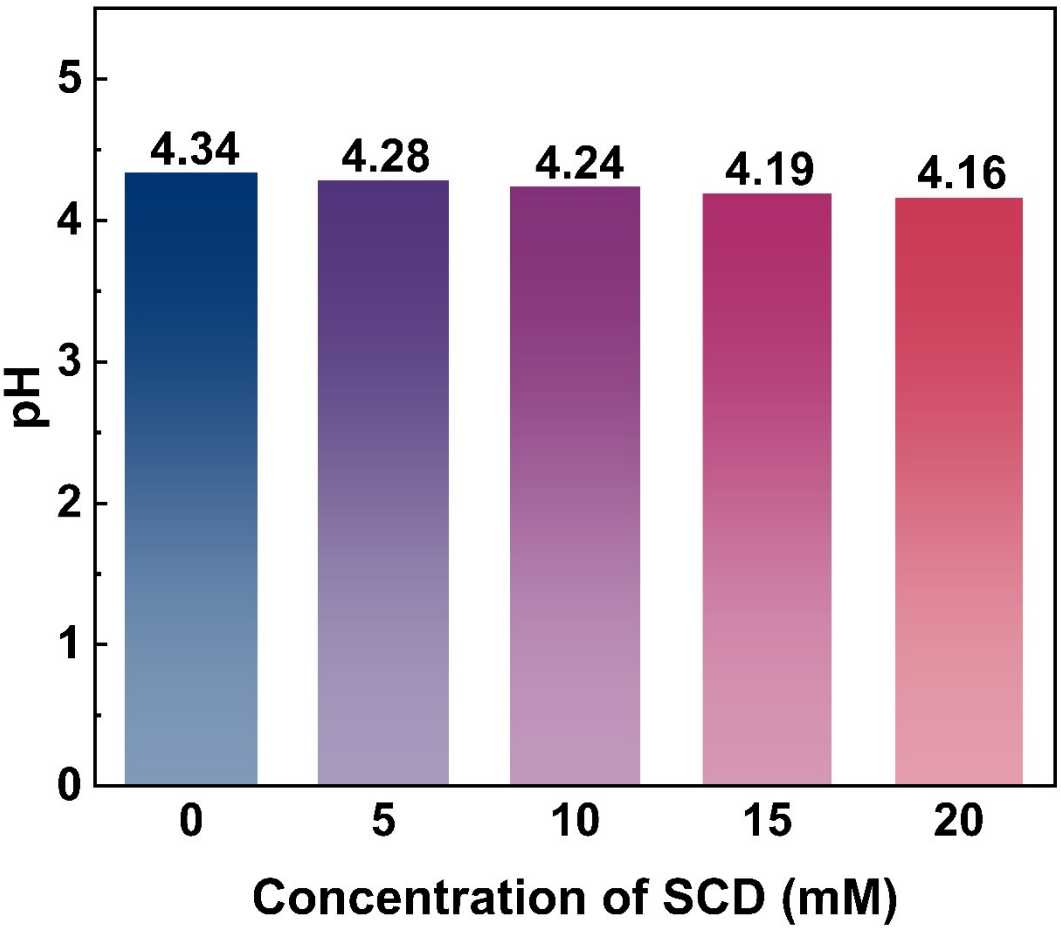

Figure S9. pH value of the electrolytes with various SCD concentrations.

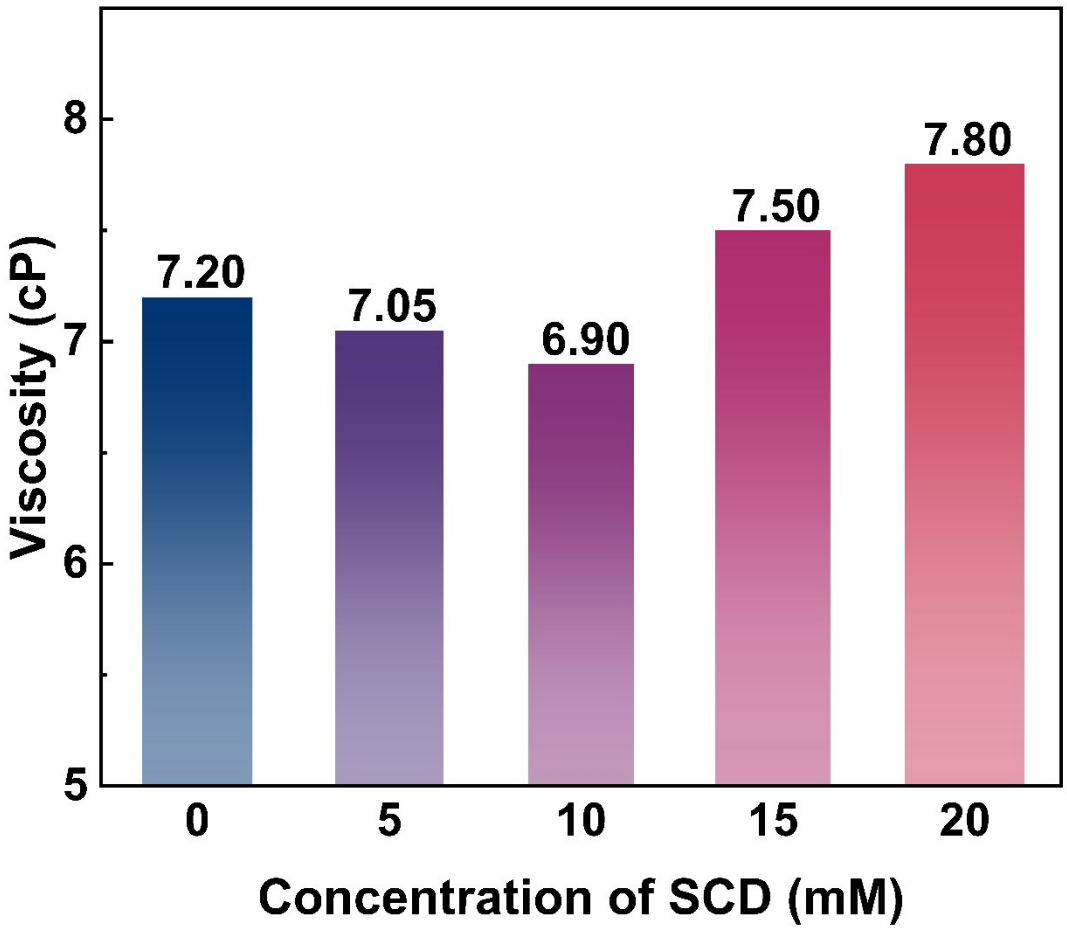

Figure S10. Viscosity of the electrolytes with various SCD concentrations.

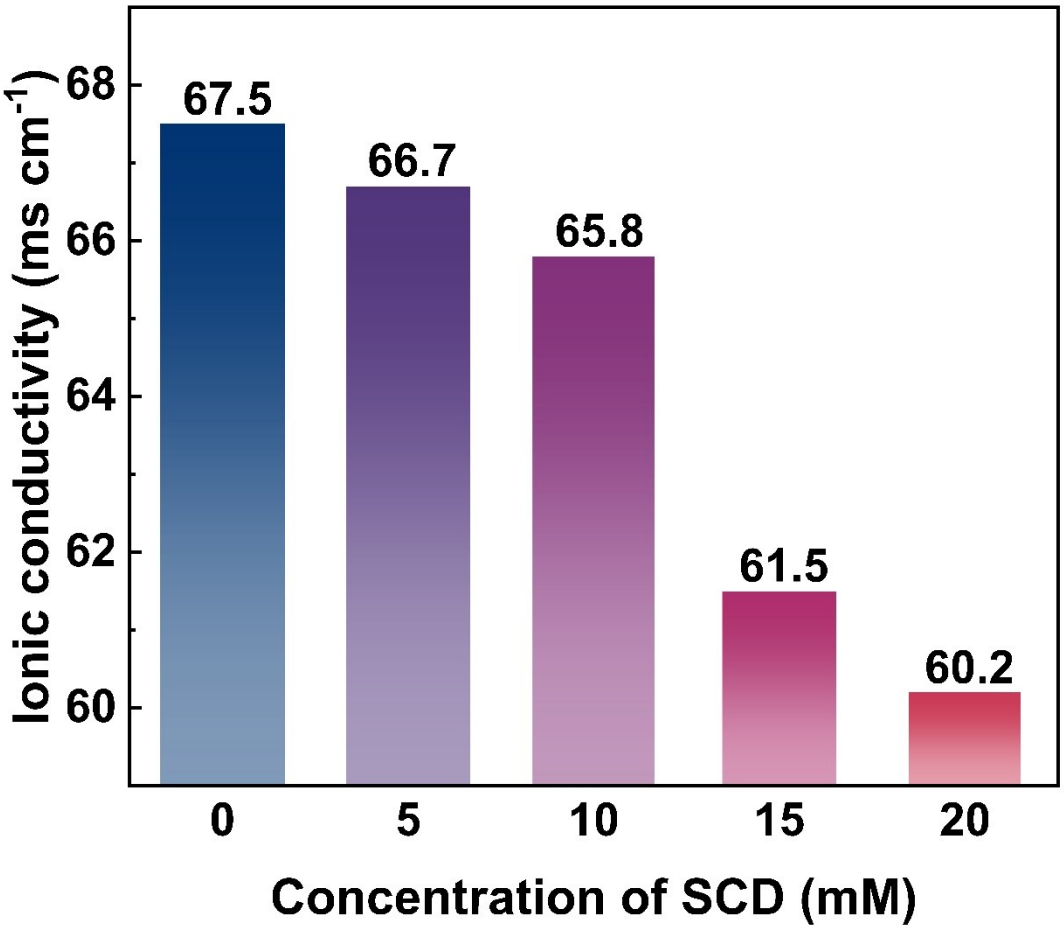

Figure S11. Ionic conductivity of the electrolytes with various SCD concentrations.

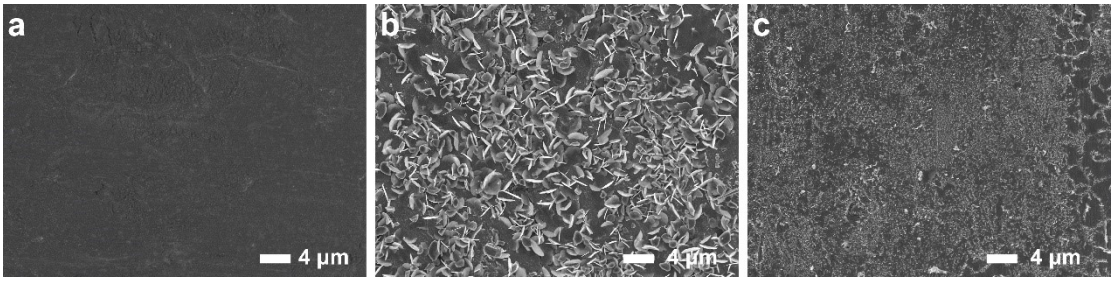

Figure S12. Surface morphologies of a) Zn plate and the Zn plates after immersed in b) ZS and c) ZS + SCD electrolytes for 3 days.

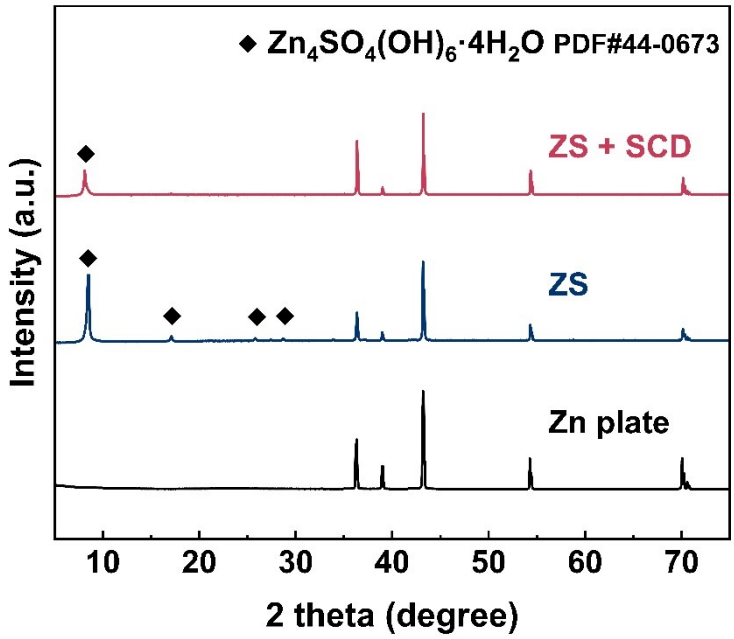

Figure S13.XRD patterns of Zn plate and the Zn plates after immersed in ZS and ZS + SCD electrolytes for 3 days.

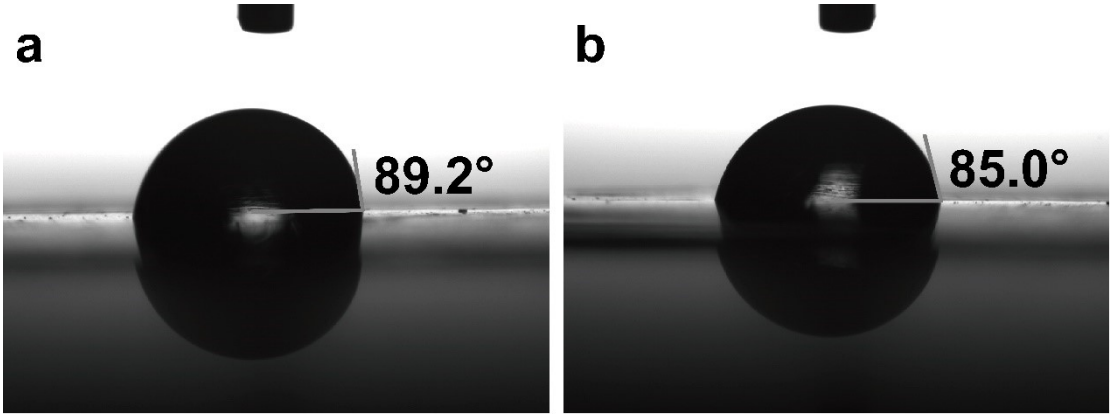

Figure S14. Contact angle of the a) ZS and b) ZS + SCD electrolytes on Zn surface.

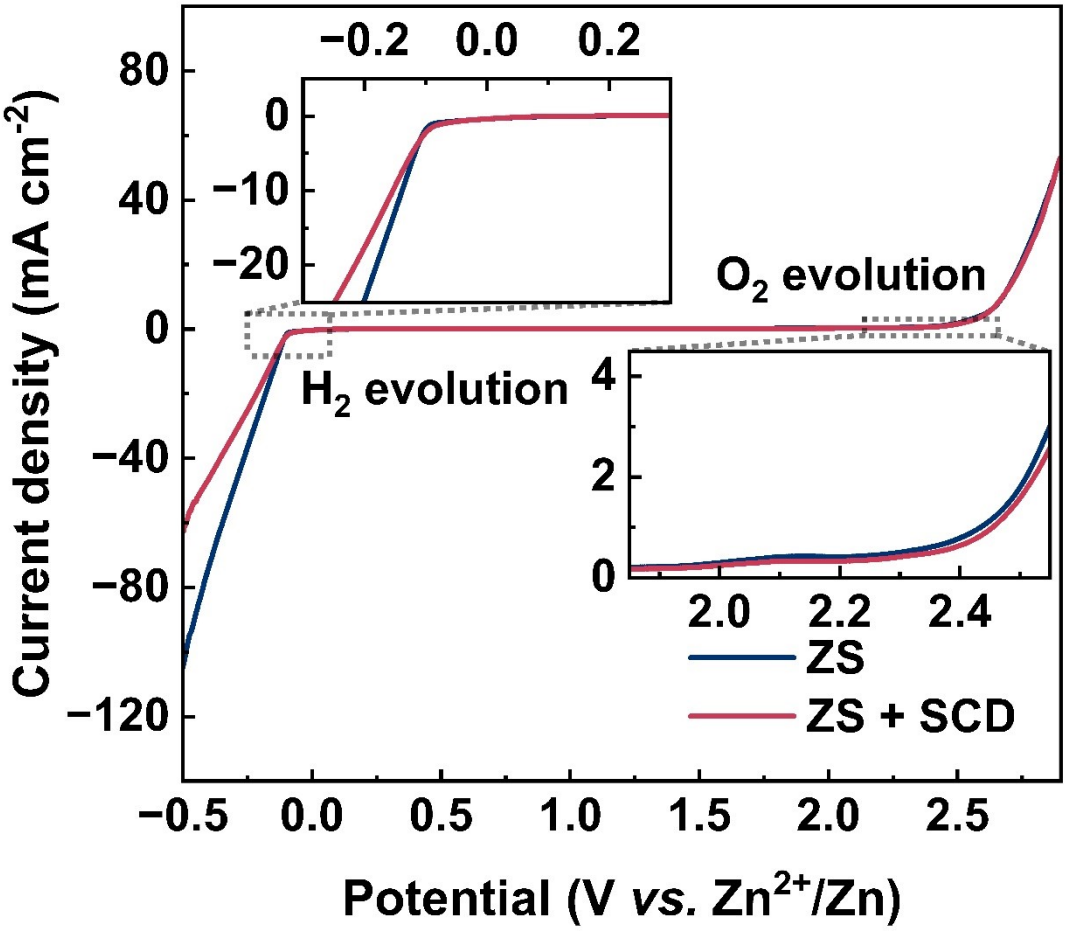

Figure S15. Electrochemical stability window of ZS and ZS + SCD electrolytes.

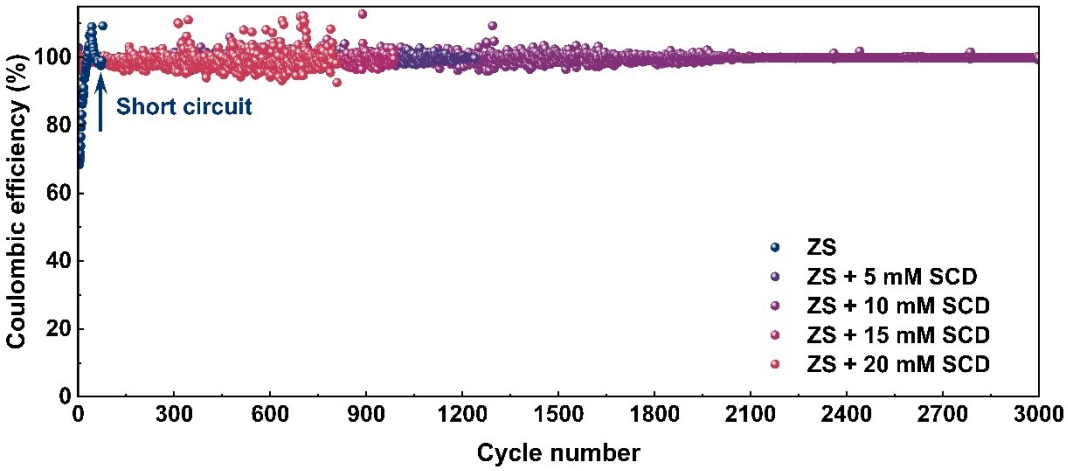

Figure S16. Coulombic efficiency (CE) of the Zn//Cu asymmetric cells using different electrolytes.

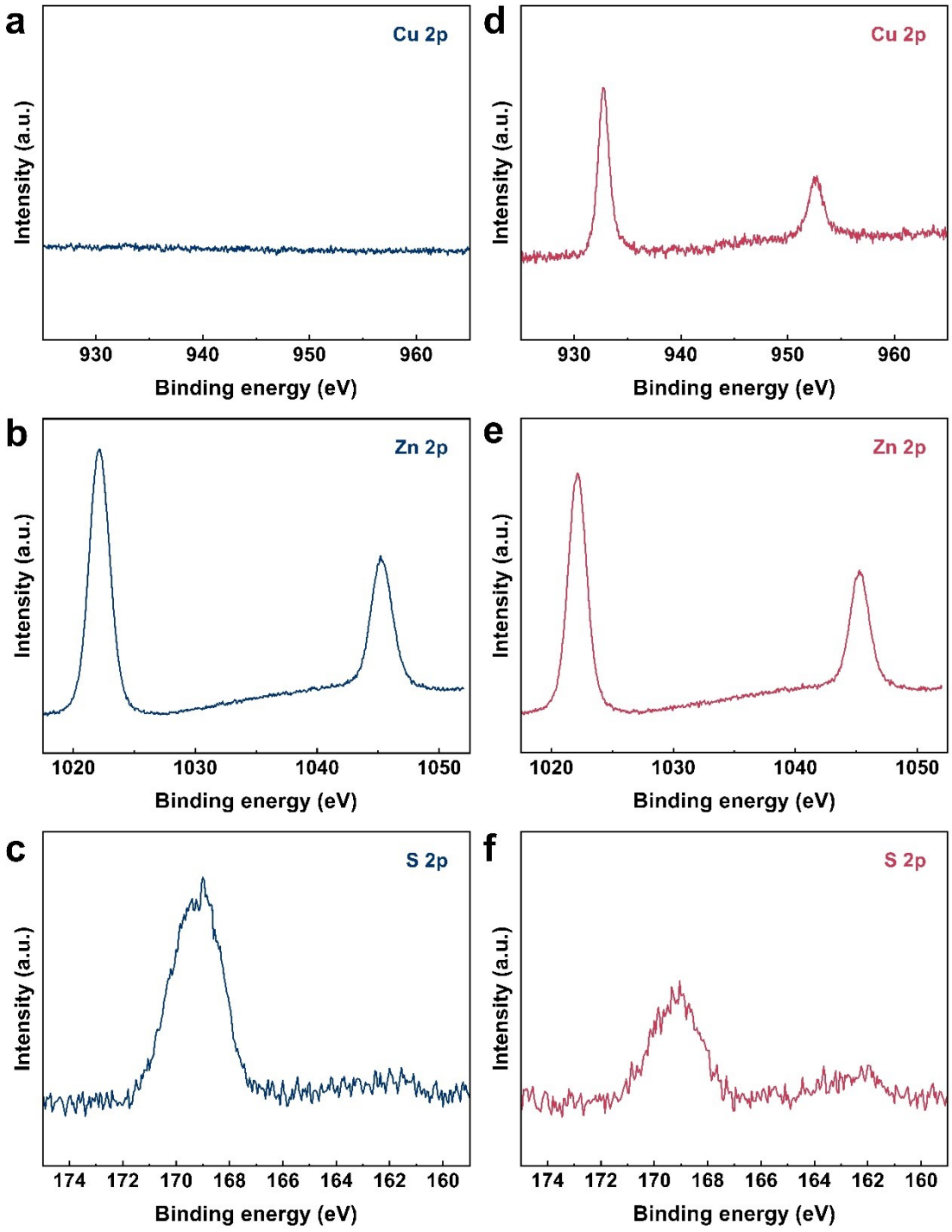

Figure S17. Cu 2p, Zn 2p, and S 2p XP spectra of the Cu surface a-c) before and d-f) after the voltage peak in the charging process of Zn//Cu asymmetric cell using ZS + SCD electrolyte.

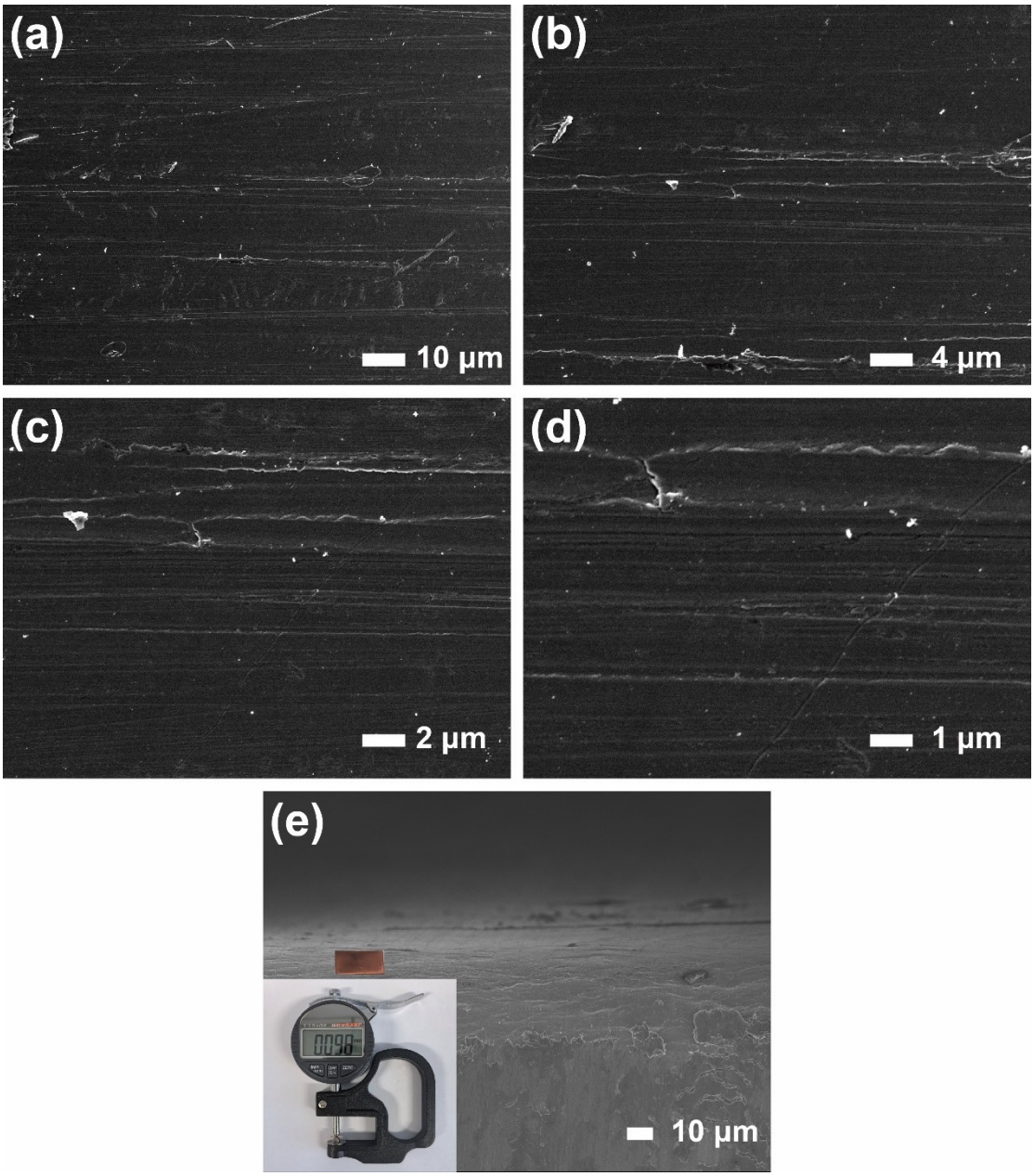

Figure S18. The a-d) surface and e) cross-section morphologies of Cu plate, inset: the thickness measured by digital micrometer.

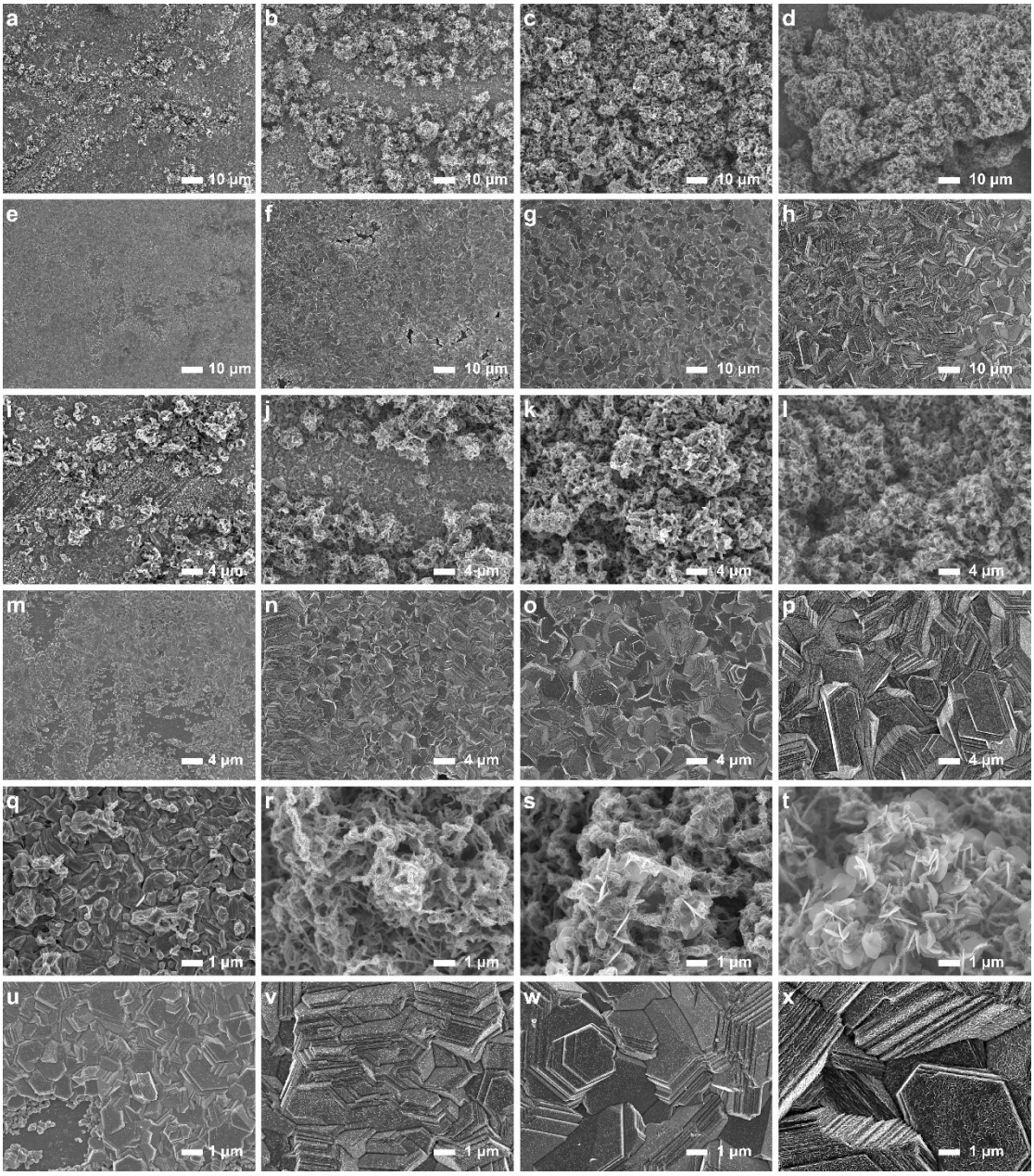

Figure S19. Surface morphologies of deposited Zn in ZS (the 1st, 3rd and 5th row) and ZS + SCD (the 2nd, 4th and 6th row) electrolytes at 5 mA cm^{-2} with various areal capacities under different magnifications. The deposition capacities are 0.5, 1, 2.5, 5 mAh cm^{-2}, and the magnifications are 1000, 2500 and 10000, respectively.

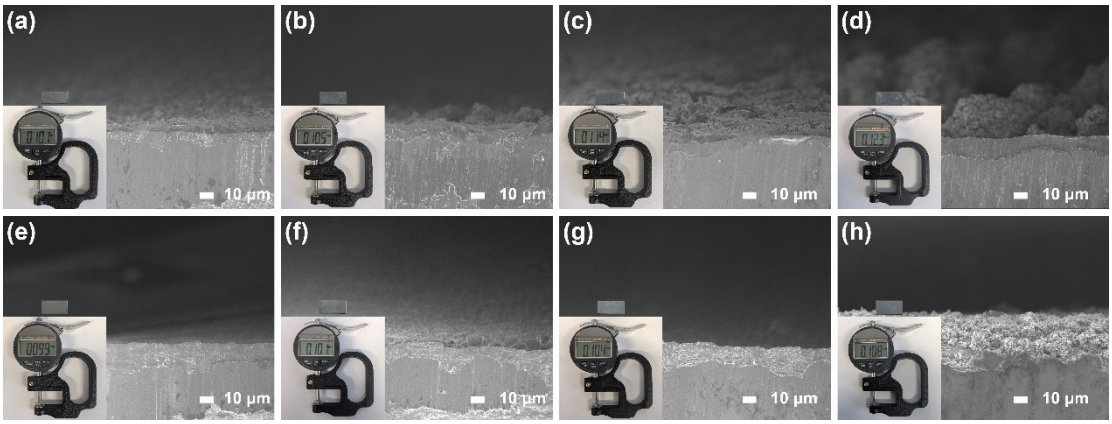

Figure S20. Cross-section morphologies of deposited Zn in a-d) ZS and e-f) ZS + SCD electrolytes at 5 mA cm^{-2} with various areal capacities. Inset: the thickness measured by digital micrometer. The deposition capacities are 0.5, 1, 2.5, 5 mAh cm^{-2}, respectively.

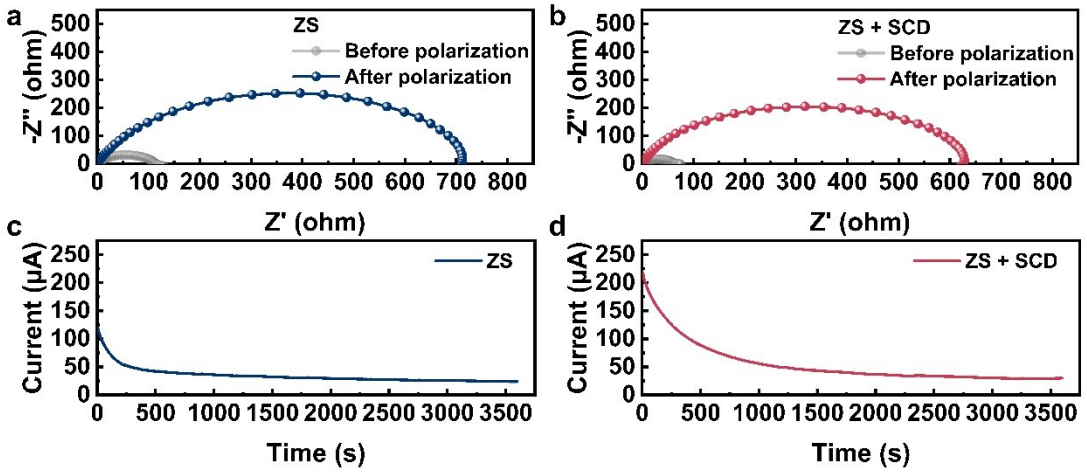

Figure S21. The EIS and polarization measurements for calculating the Zn^{2+} transference number. The EIS spectra of the Zn//Zn symmetric cells using a) ZS and b) ZS + SCD electrolytes before and after polarization, and c-d) corresponding i-t curves at ΔV = 20 mV polarization.

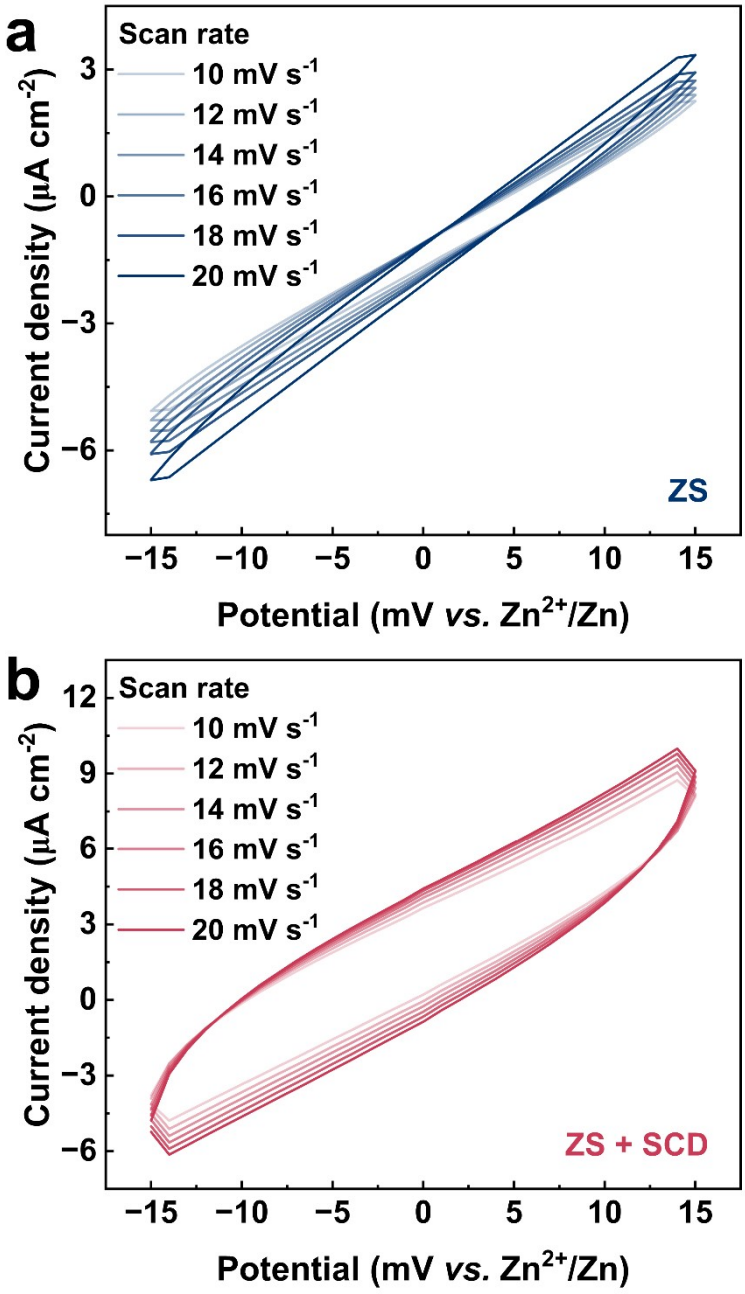

Figure S22. CV curves of Zn//Zn symmetric cells using a) ZS and b) ZS + SCD electrolytes with a voltage range from -15 to 15 mV at various scan rates.

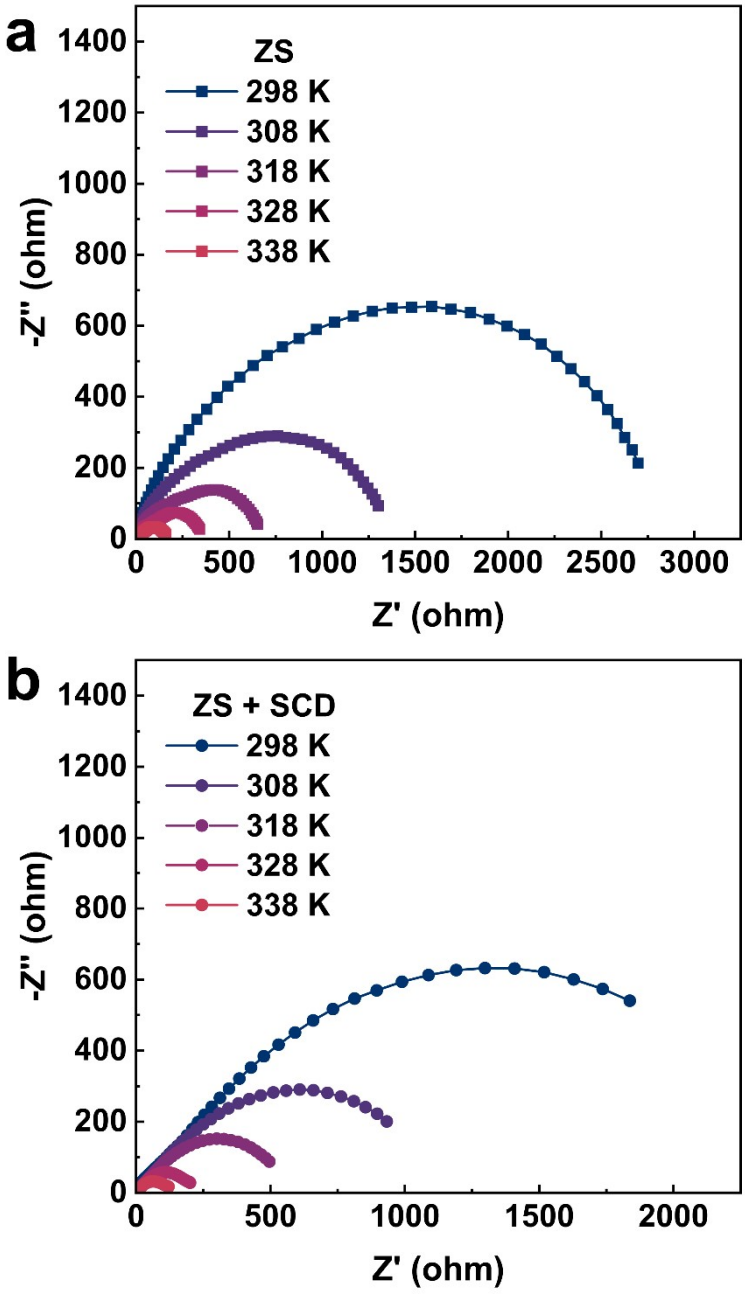

Figure S23. EIS spectra of Zn//Zn symmetric cells using a) ZS and b) ZS + SCD electrolytes under various temperatures.

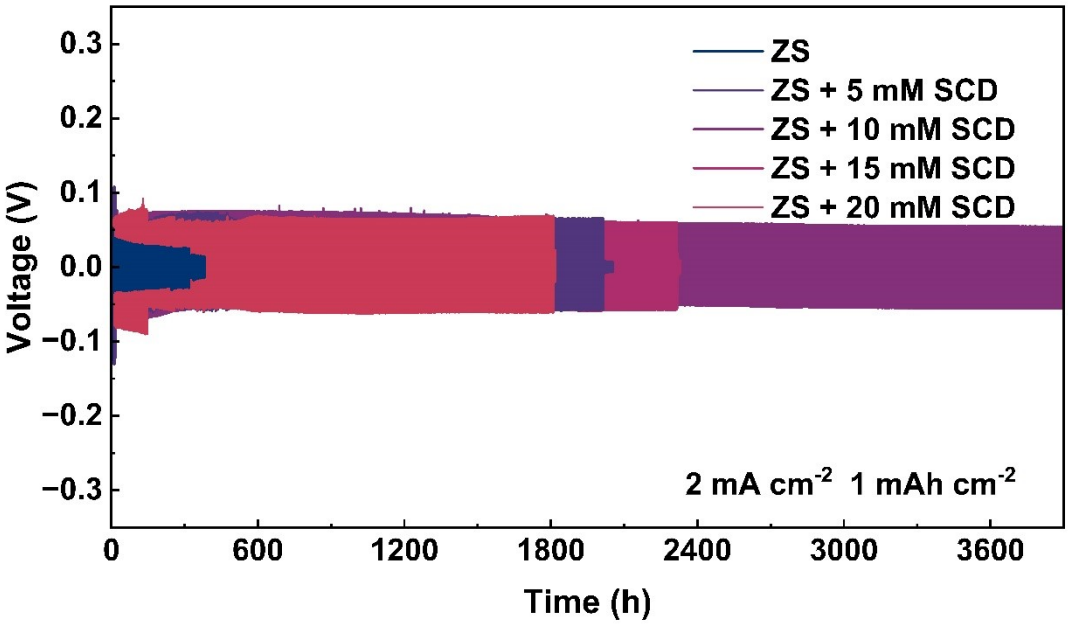

Figure S24. Cycling performance of Zn//Zn symmetric cells using different electrolytes at 2 mA cm^{-2} with a capacity of 1 mAh cm^{-2}.

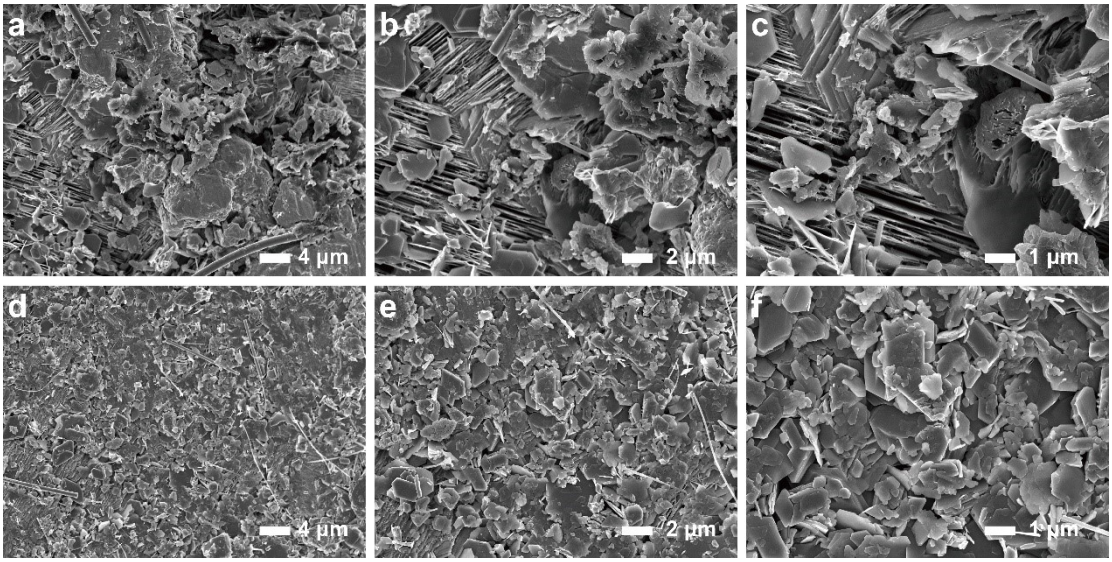

Figure S25. Surface morphologies of Zn surface in a-c) ZS and d-f) ZS + SCD electrolytes after 100 cycles at 2 mA cm^{-2} with a capacity of 1 mA cm^{-2}.

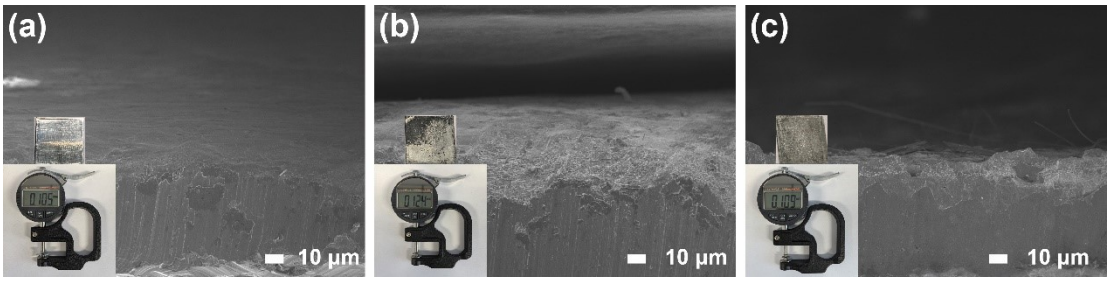

Figure S26. Cross-section morphologies of a) Zn plate and Zn surface in b) ZS and c) ZS + SCD electrolytes after 100 cycles at 2 mA cm^{-2} with a capacity of 1 mA cm^{-2}, inset: the thickness measured by digital micrometer.

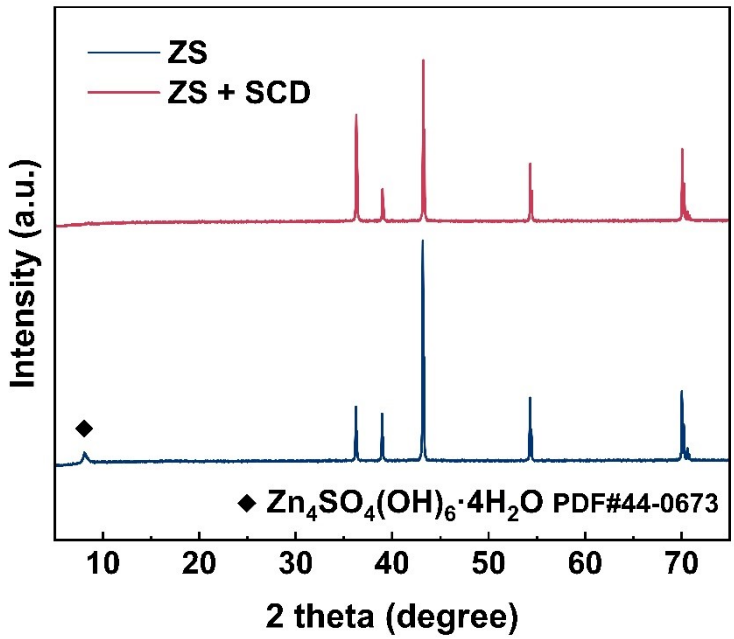

Figure S27. XRD patterns of Zn surface in ZS and ZS + SCD electrolytes after 100 cycles at 2 mA cm^{-2} with a capacity of 1 mA cm^{-2}.

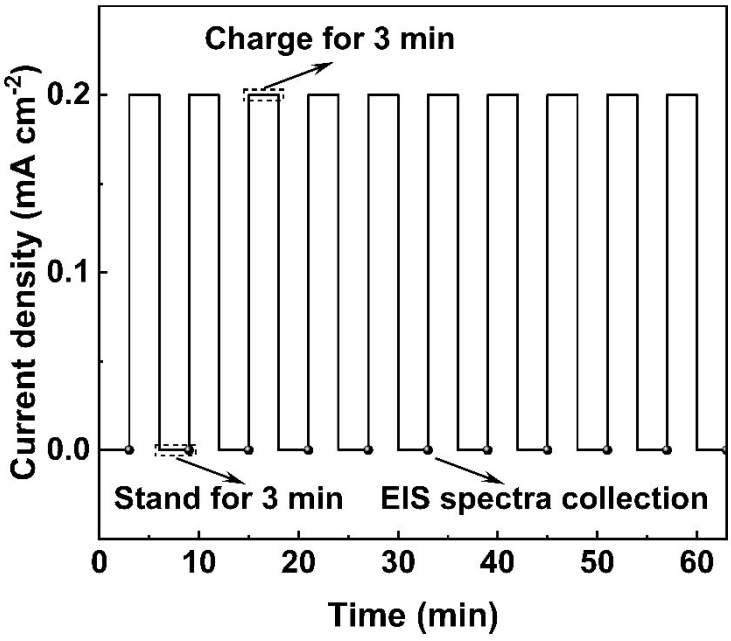

Figure S28. Schematic illustration of in-situ EIS measurements.

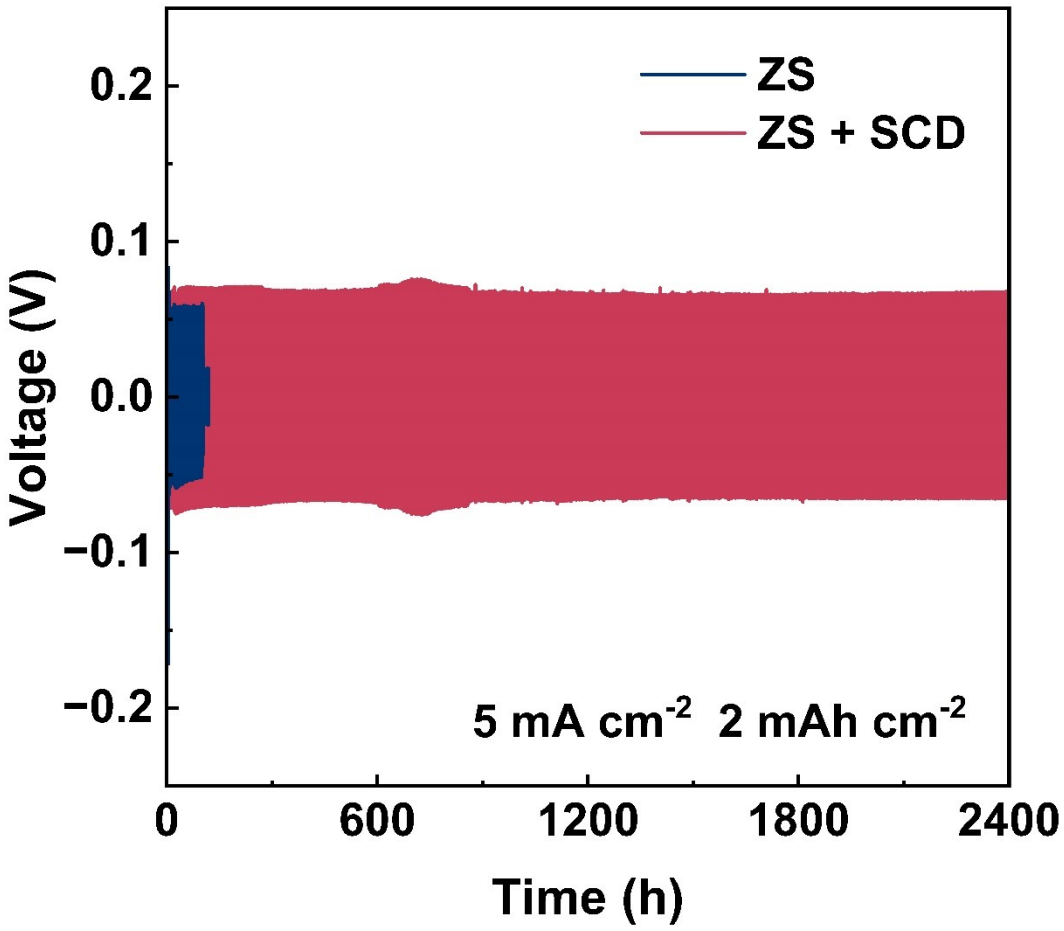

Figure S29. Cycling performance of Zn//Zn symmetric cells using ZS and ZS + SCD electrolytes at 5 mA cm^{-2} with a capacity of 2 mAh cm^{-2}.

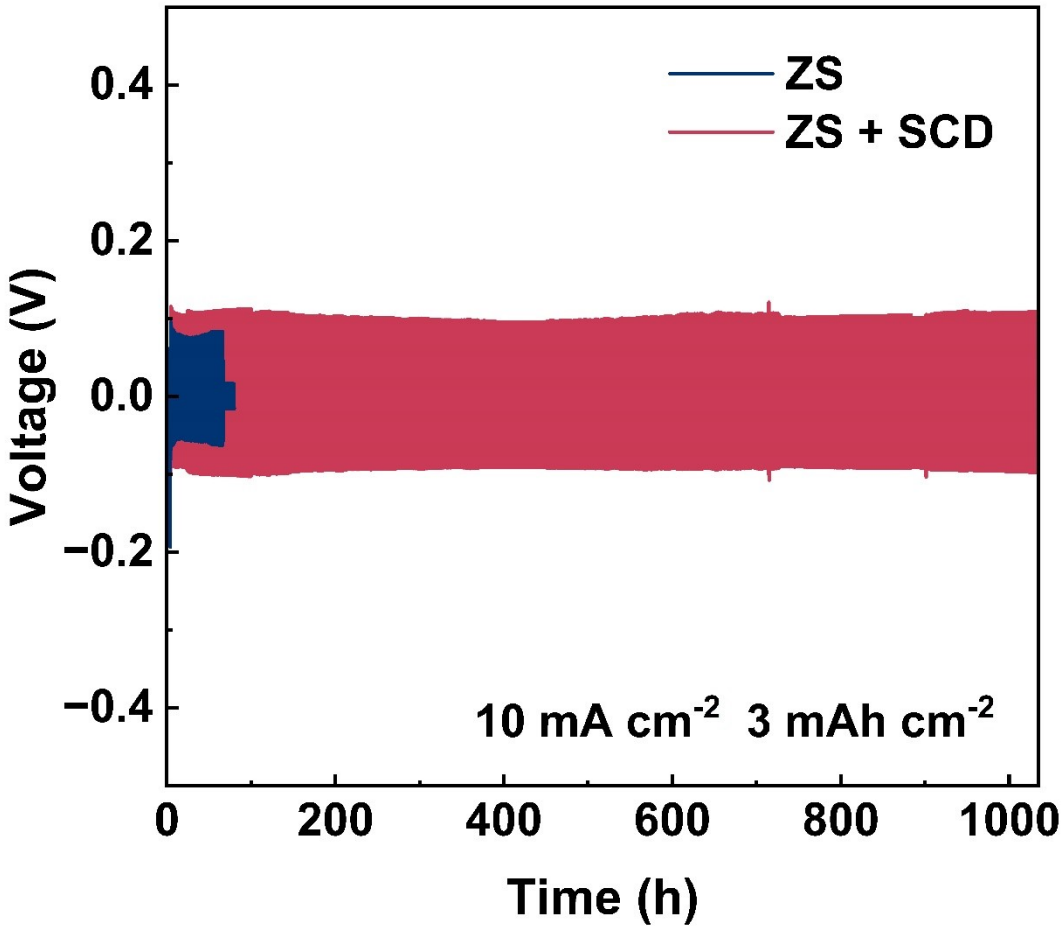

Figure S30. Cycling performance of Zn//Zn symmetric cells using ZS and ZS + SCD electrolytes at 10 mA cm^{-2} with a capacity of 3 mAh cm^{-2}.

Figure S31. The Zn foil used in the DOD test with a thickness of ~ 9 μm.

Figure S32. The Zn foil used in the DOD test with a thickness of ~ 25 μm.

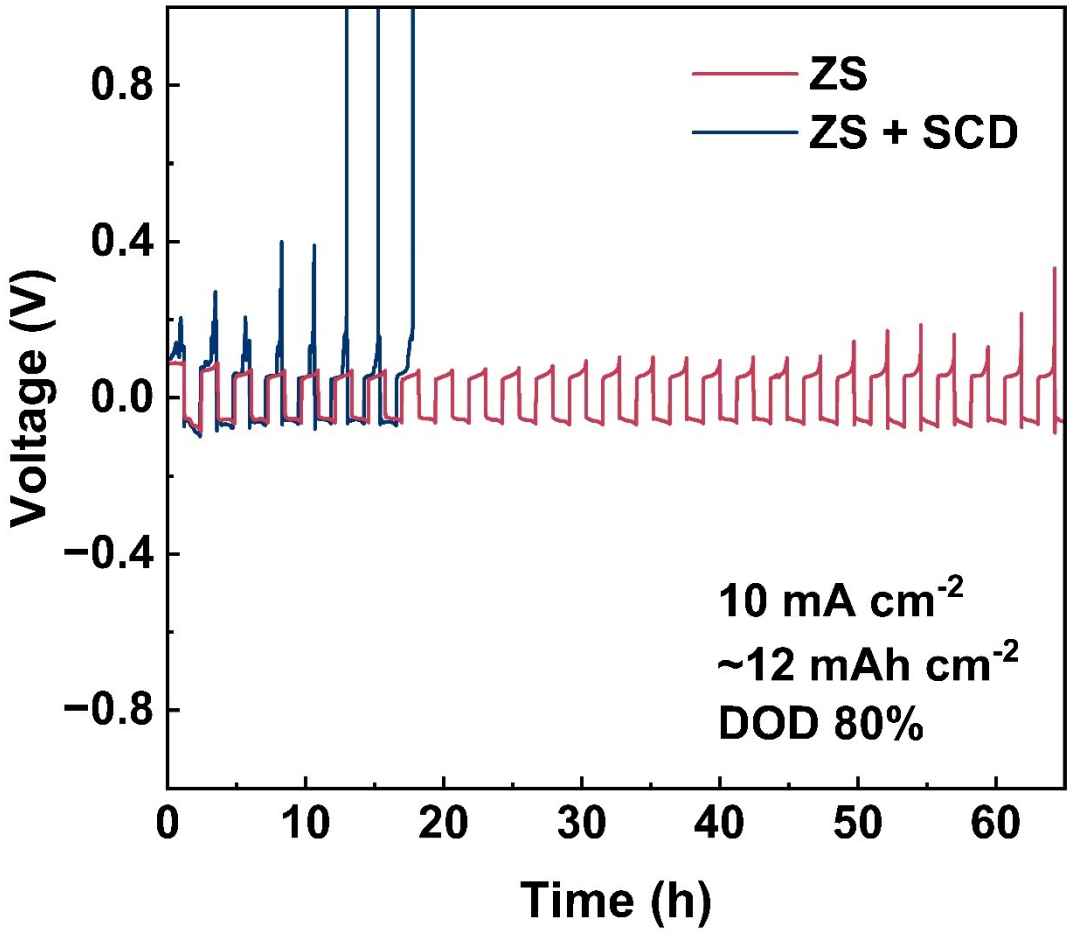

Figure S33. Cycling performance of Zn//Zn symmetric cells using ZS and ZS + SCD electrolytes at 10 mA cm^{-2} under 80% DOD with a Zn anode thickness of ~ 25 μm.

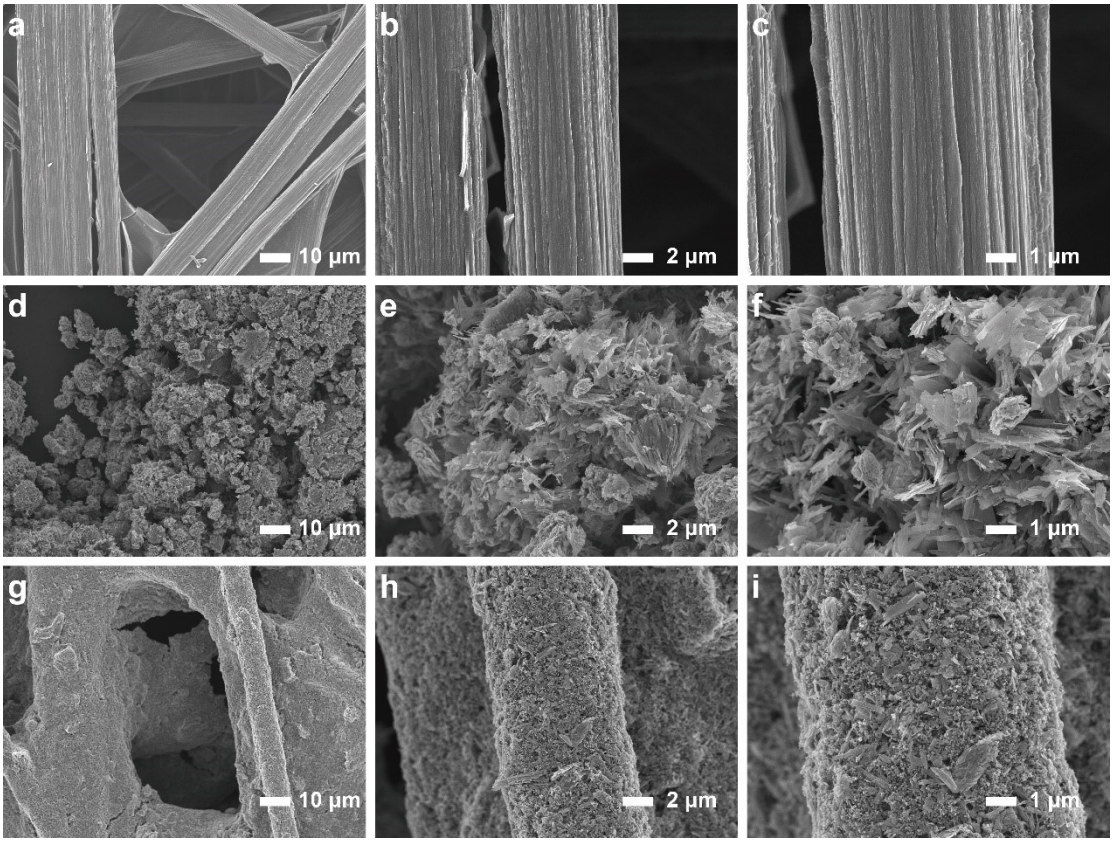

Figure S34. SEM images of a-c) carbon paper, d-f) $NH_4V_4O_{10}$ powder and g-i) $NH_4V_4O_{10}$@CP cathode.

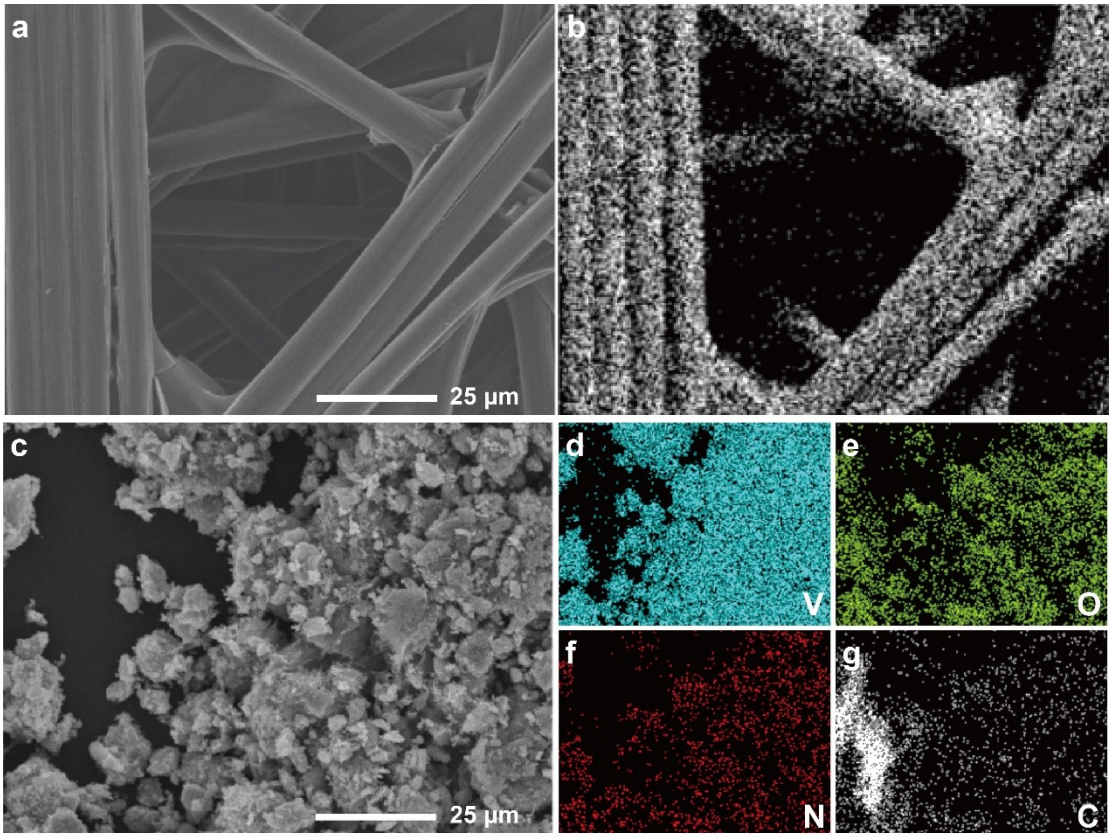

Figure S35. EDX mapping and elemental distribution of a-b) carbon paper and c-g) $NH_4V_4O_{10}$ powder.

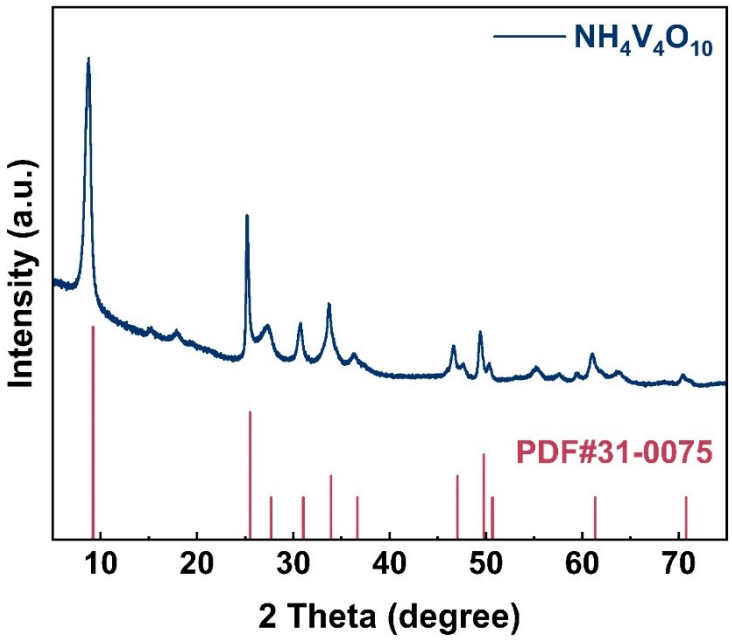

Figure S36. XRD patterns of $NH_4V_4O_{10}$ powder.

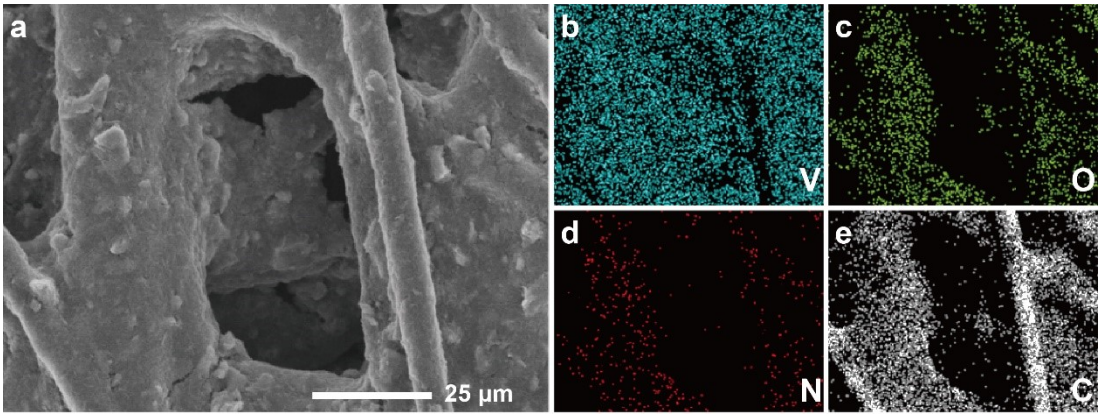

Figure S37. EDX mapping and elemental distribution of $NH_4V_4O_{10}$@CP cathode.

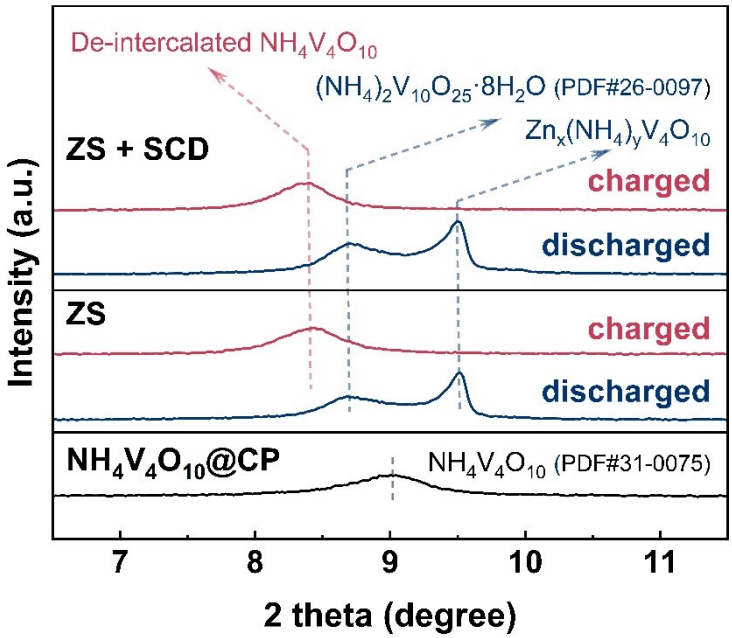

Figure. S38. XRD patterns of the cathode materials after discharged and charged in ZS and ZS + SCD electrolytes.

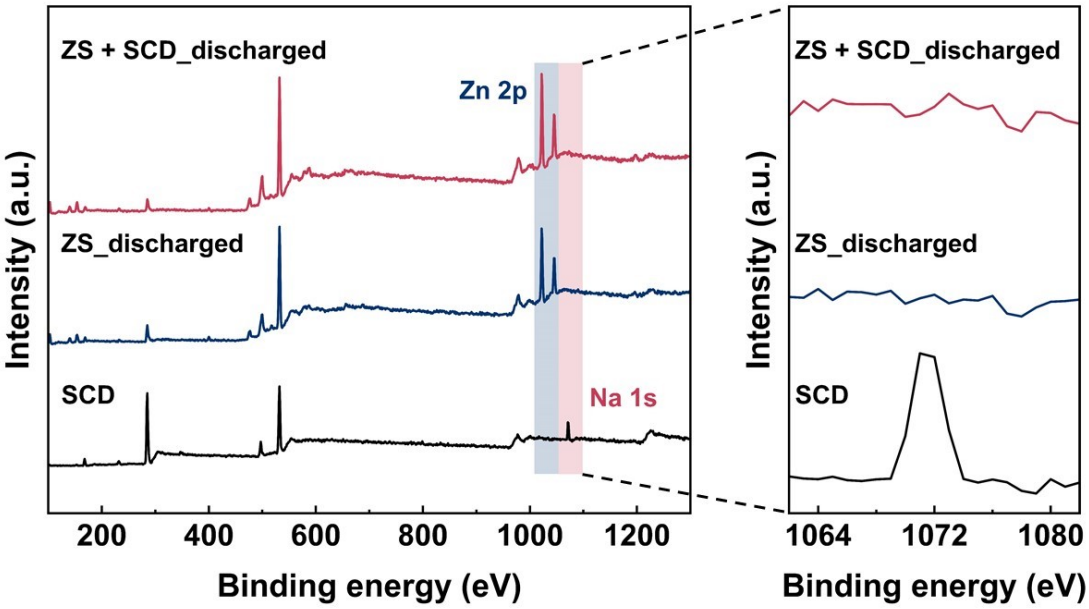

Figure S39. XP spectra of SCD powder, and the cathode discharged in ZS and ZS + SCD electrolytes.

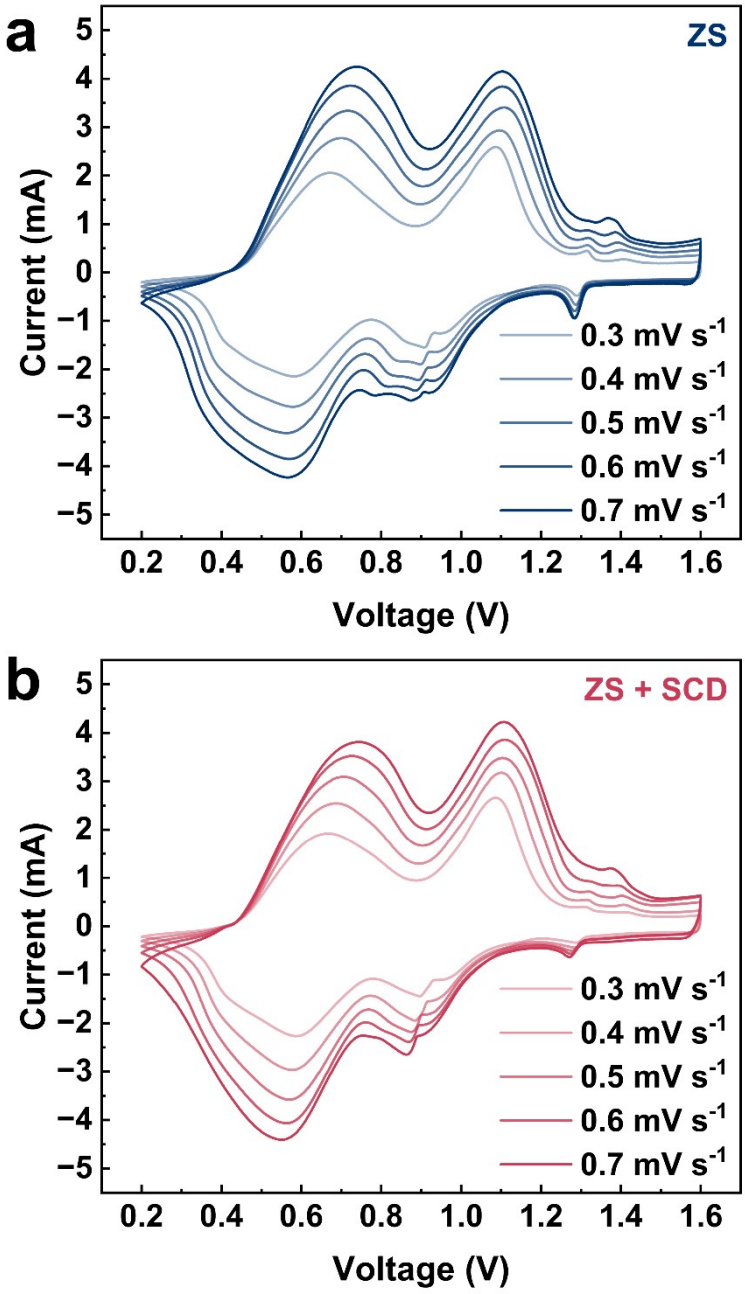

Figure S40. CV curves of Zn// $NH_4V_4O_{10}$ full cells using a) ZS and b) ZS + SCD electrolytes at various scan rates.

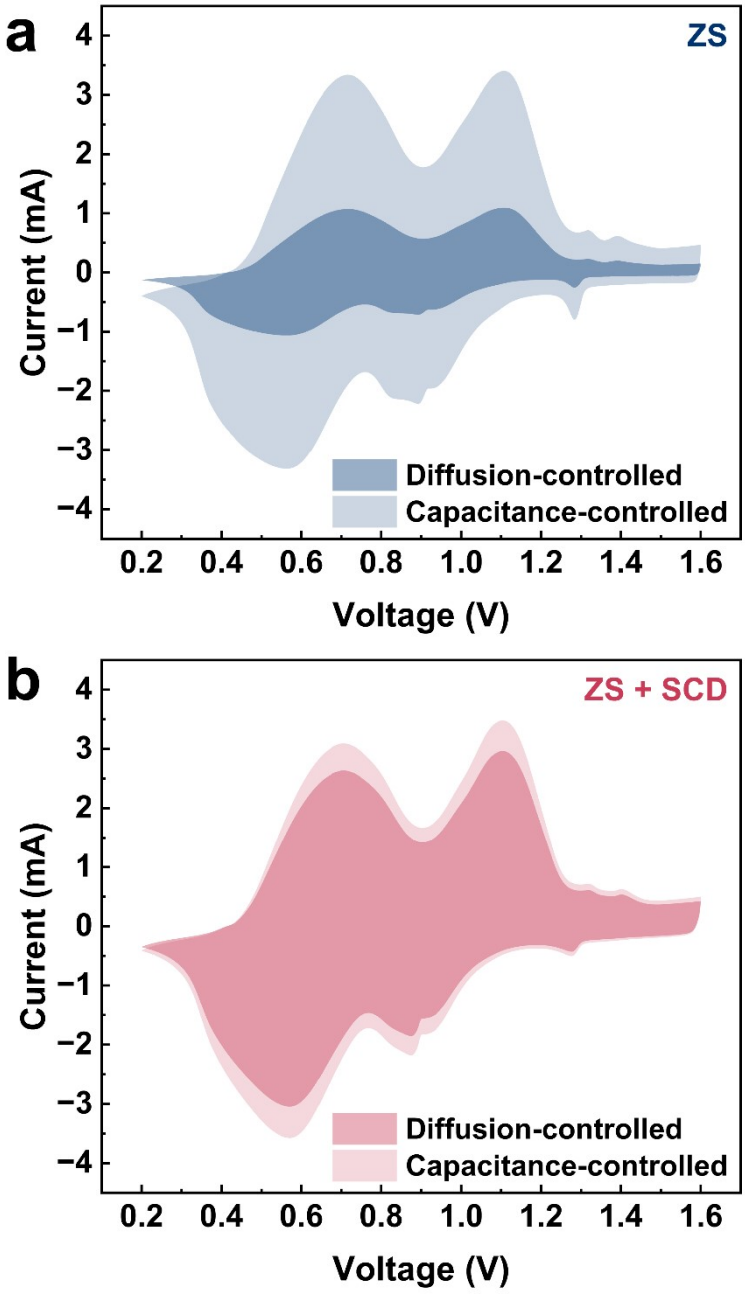

Figure S41. Representative contribution ratio of diffusion-controlled and capacitance-controlled capacity at 0.5 mV s^{-1}.

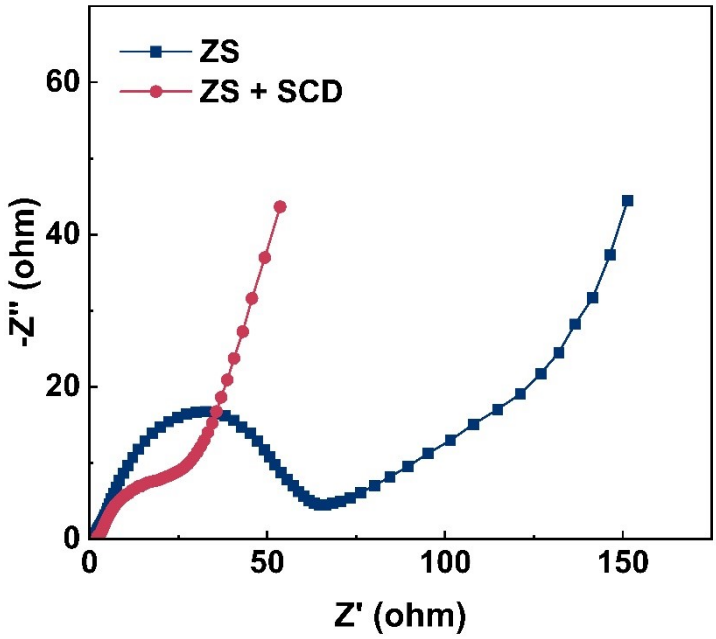

Figure S42. EIS spectra of Zn//$NH_4V_4O_{10}$ full cells using ZS and ZS + SCD electrolytes.

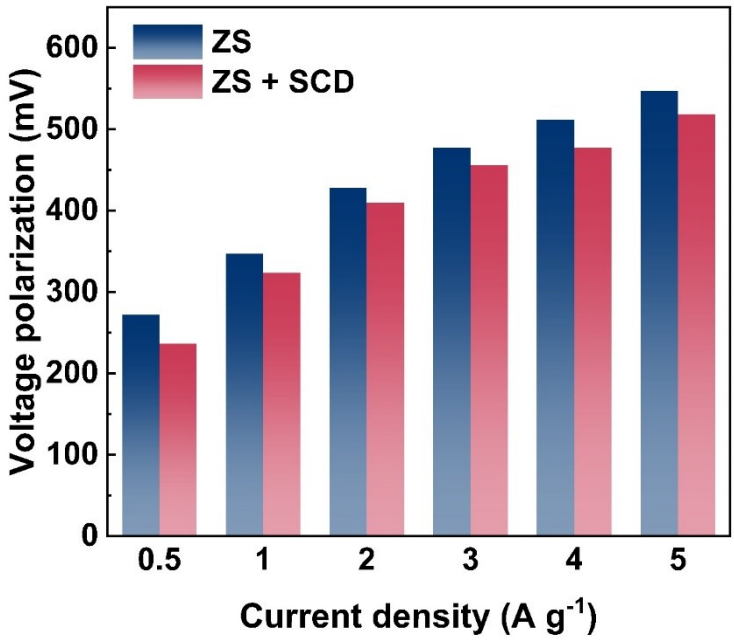

Figure S43. Comparison of the voltage polarizations of the galvanostatic charge/discharges curves of the Zn//$NH_4V_4O_{10}$ full cells using ZS and ZS + SCD electrolytes.

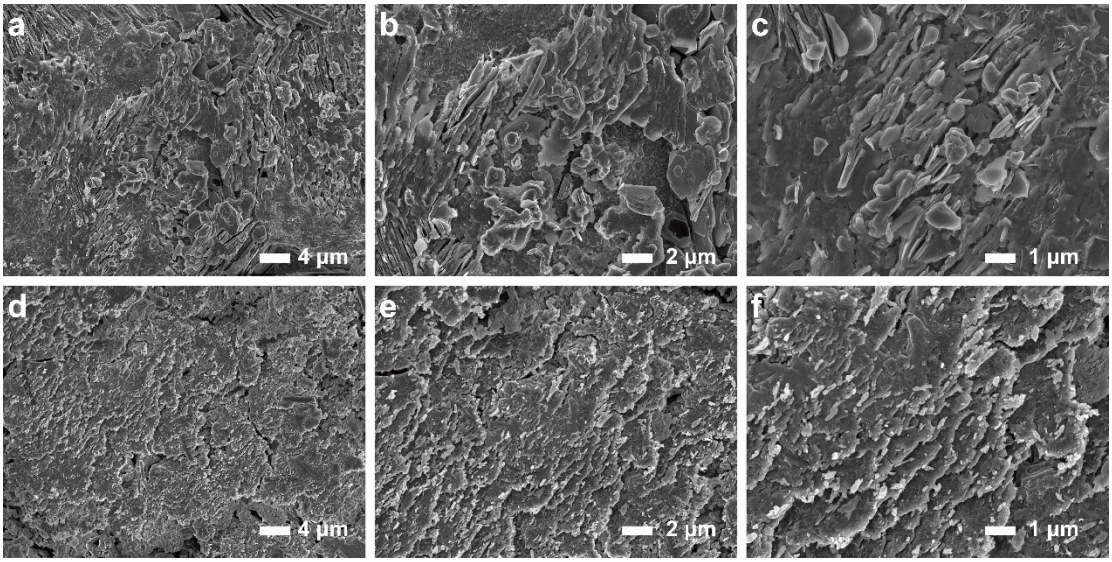

Figure S44. Surface morphologies of Zn surface in Zn//$NH_4V_4O_{10}$ full cells using a-c) ZS and d-f) ZS + SCD electrolytes after 500 cycles at 5 A g^{-1}.

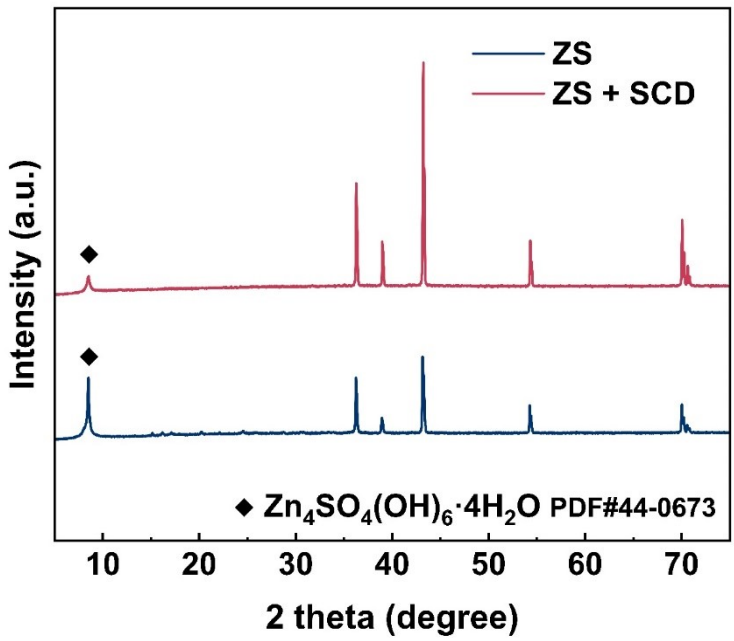

Figure S45. XRD patterns of Zn surface in Zn//$NH_4V_4O_{10}$ full cells using ZS and ZS + SCD electrolytes after 500 cycles at 5 A g^{-1}.

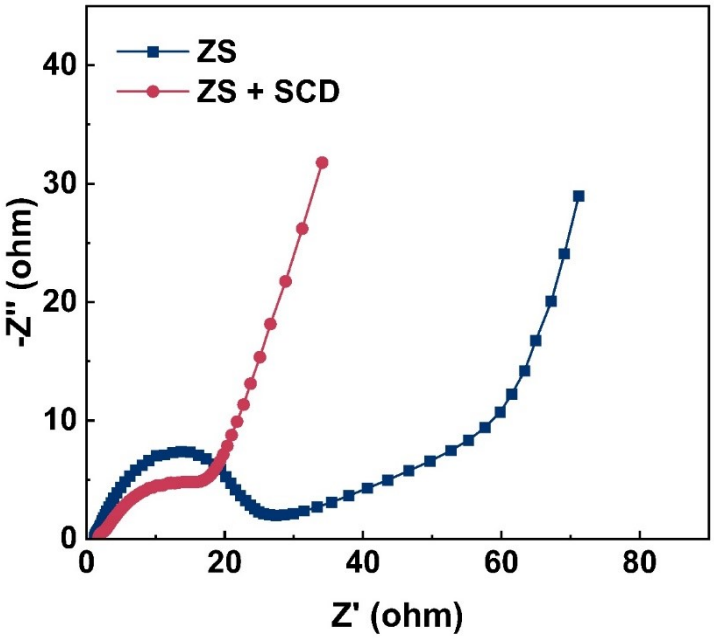

Figure S46. EIS spectra of Zn//$NH_4V_4O_{10}$ full cells using ZS and ZS + SCD electrolytes after 500 cycles at 5 A g^{-1}.

Table S1. Performance comparison of Zn//Zn symmetric cells with SCD and previously reported additives.

Additives	Current density (mA cm^{-2})	Areal capacity (mAh cm^{-2})	Lifespan (h)	Cumulative plating capacity (Ah cm^{-2})	DOD	Refs
α-CD	5	5	200	0.5	30%	15
	10	1	160	0.8	6%	
β-CD	4	2	1700	3.4	6.8%	16
β-CD @ClO_4^-	1	1	1000	0.5	-	17
	5	5	350	0.875	-	
	-	-	145	0.875	30%	
$La(NO_3)_3$	1	1	1200	0.6	2.1%	18
ZnF_2	1	1	600	0.3	-	19
Vanilli	1	1	1000	0.5	6.8%	20
Glutamine	3	3	700	1.05	-	21
TDFND	1	1	1250	0.625	1.7%	22
	5	5	520	1.3	8.5%	
	10	5	430	2.15	17.1%	
C_3N_4 QD	1	1	1200	0.6	0.85%	23
Taurine	10	5	250	1.25	-	24
Glycine	1	0.5	2000	1	-	25
	4	2	600	1.2	-	
TA-Na	5	2.5	430	1.075	4.3%	26
HMT	2	2	1200	1.2	-	27
TXA	5	5	700	1.75	-	28
PA	2	1	1000	1	1.7%	29
TH	5	1	700	1.75	1.7%	30
18C6	1	1	2400	1.2	-	31
SeO_2	2	2	2100	2.1	3.4%	32
TU	10	1	600	3	-	33
DA	10	10	200	1	28.5%	34
Glycine	5	1	700	1.75	-	35
CNPM	5	1	750	1.875	-	36
PEG	2	1	400	0.4	-	37
Glucose	1	1	2000	1	1.7%	38
Cys	5	5	620	1.55	17.1%	39
MSG	10	10	520	2.6	-	40
Cit	1	1	1700	0.85	3.4%	41
	5	5	1200	3	17.1%	
	10	10	650	3.25	34.2%	

PASP	20	1	200	2	3.4%	42
NTA	10	2	500	2.5	-	43
Sucrose	10	10	625	3.125	17.1%	44
[EMIm]OTf	5	5	1100	2.75	8.5%	45
	10	10	600	3	17.1%	
D-Arabinose	10	1	700	3.5	1.7%	46
THF	1	1	2800	1.4	-	47
HPA	20	5	300	3	12.2%	48
GPC	1	4	1450	0.725	45.3%	49
DM	5	2	840	2.1	3.4%	50
Pectin	5	5	900	2.25	28.5%	51
	2	2	2200	2.2	11.4%	
	1	1	2600	1.3	5.7%	
SCD	**2**	**1**	**3900**	**3.9**	**1.7%**	**Our work**
	5	**2**	**2400**	**6.0**	**3.4%**	
	10	**3**	**1035**	**5.175**	**5.1%**	
	5	**3**	**500**	**1.25**	**51.3%**	
	10	**10**	**280**	**1.4**	**68%**	

References

1 G. Kresse, J. Furthmüller, *Comput. Mater. Sci.*, 1996, **6**, 15-50.
2 G. Kresse, J. Furthmüller, *Phys. Rev. B*, 1996, **54**, 11169-11186.
3 J. P. Perdew, K. Burke, M. Ernzerhof, *Phys. Rev. Lett.*, 1996, **77**, 3865−3868.
4 G. Kresse, D. Joubert, *Phys. Rev. B*, 1999, **59**, 1758-1775.
5 P. E. Blöchl, *Phys. Rev. B*, 1994, **50**, 17953-17979.
6 H. J. Monkhorst, J. D. Pack, *Phys. Rev. B*, 1976, **13**, 5188-5192.
7 S. Grimme, J. Antony, S. Ehrlich, H. Krieg, *J. Chem. Phys.*, 2010, **132**.
8 S. Grimme, S. Ehrlich, L. Goerigk, *J. Comput. Chem.*, 2011, **32**, 1456-1465.
9 A. D. Becke, *J. Chem. Phys.*, 1993, **98**, 5648-5652.
10 S. Miertuš, E. Scrocco, J. Tomasi, *Chem. Phys.*, 1981, **55**, 117-129.
11 A. V. Marenich, C. J. Cramer, D. G. Truhlar, *J. Phys. Chem. B*, 2009, **113**, 6378-6396.
12 T. Lu, F. Chen, *J. Comput. Chem.*, 2011, **33**, 580-592.
13 W. Humphrey, A. Dalke, K. Schulten, *J. Mol. Graph.*, 1996, **14**, 33-38.
14 D. Van Der Spoel, E. Lindahl, B. Hess, G. Groenhof, A. E. Mark, H. J. C. Berendsen, *J. Comput. Chem.*, 2005, **26**, 1701-1718.
15 K. Zhao, G. Fan, J. Liu, F. Liu, J. Li, X. Zhou, Y. Ni, M. Yu, Y.-M. Zhang, H. Su, Q. Liu, F. Cheng, *J. Am. Chem. Soc.*, 2022, **144**, 11129-11137.
16 C. Meng, W. He, L. Jiang, Y. Huang, J. Zhang, H. Liu, J. J. Wang, *Adv.*

Funct. Mater., 2022, **32**, 2207732.
17 M. Qiu, P. Sun, Y. Wang, L. Ma, C. Zhi, W. Mai, *Angew. Chem. Int. Ed.*, 2022, **61**, e202210979.
18 R. Zhao, H. Wang, H. Du, Y. Yang, Z. Gao, L. Qie, Y. Huang, *Nat. Commun.*, 2022, **13**, 3252.
19 Y. An, Y. Tian, K. Zhang, Y. Liu, C. Liu, S. Xiong, J. Feng, Y. Qian, *Adv. Funct. Mater.*, 2021, **31**, 2101886.
20 K. Zhao, F. Liu, G. Fan, J. Liu, M. Yu, Z. Yan, N. Zhang, F. Cheng, *ACS Appl. Mater. Interfaces*, 2021, **13**, 47650-47658.
21 J. Yin, M. Li, X. Feng, T. Cui, J. Chen, F. Li, M. Wang, Y. Cheng, S. Ding, X. Xu, J. Wang, *J. Mater. Chem. A*, 2024, **12**, 1543-1550.
22 T. Li, S. Hu, C. Wang, D. Wang, M. Xu, C. Chang, X. Xu, C. Han, *Angew. Chem. Int. Ed.*, 2023, **62**, e202314883.
23 W. Zhang, M. Dong, K. Jiang, D. Yang, X. Tan, S. Zhai, R. Feng, N. Chen, G. King, H. Zhang, H. Zeng, H. Li, M. Antonietti, Z. Li, *Nat. Commun.*, 2022, **13**, 5348.
24 K. Ouyang, S. Chen, W. Ling, M. Cui, Q. Ma, K. Zhang, P. Zhang, Y. Huang, *Angew. Chem. Int. Ed.*, 2023, **62**, e202311988.
25 Q. Gou, H. Luo, Q. Zhang, J. Deng, R. Zhao, O. Odunmbaku, L. Wang, L. Li, Y. Zheng, J. Li, D. Chao, M. Li, *Small*, 2023, **19**, 2207502.
26 J. Wan, R. Wang, Z. Liu, L. Zhang, F. Liang, T. Zhou, S. Zhang, L. Zhang, Q. Lu, C. Zhang, Z. Guo, *ACS Nano*, 2023, **17**, 1610-1621.
27 X. Gu, Y. Du, Z. Cao, F. Ma, J. Li, Q. Wang, C. Lai, *Chem. Eng. J.*, 2023, **460**, 141902.
28 J. Yin, H. Liu, P. Li, X. Feng, M. Wang, C. Huang, M. Li, Y. Su, B. Xiao, Y. Cheng, X. Xu, *Energy Storage Mater.*, 2023, **59**, 102800.
29 Y. Chen, F. Gong, W. Deng, H. Zhang, X. Wang, *Energy Storage Mater.*, 2023, **58**, 20-29.
30 Z. Miao, Q. Liu, W. Wei, X. Zhao, M. Du, H. Li, F. Zhang, M. Hao, Z. Cui, Y. Sang, X. Wang, H. Liu, S. Wang, *Nano Energy*, 2022, **97**, 107145.
31 R. Li, M. Li, Y. Chao, J. Guo, G. Xu, B. Li, Z. Liu, C. Yang, YanYu, *Energy Storage Mater.*, 2022, **46**, 605-612.
32 C. Huang, X. Zhao, Y. Hao, Y. Yang, Y. Qian, G. Chang, Y. Zhang, Q. Tang, A. Hu, X. Chen, *Adv. Funct. Mater.*, 2022, **32**, 2112091.
33 P. Liu, L. Yang, B. Xiao, H. Wang, L. Li, S. Ye, Y. Li, X. Ren, X. Ouyang, J. Hu, F. Pan, Q. Zhang, J. Liu, *Adv. Funct. Mater.*, 2022, **32**, 2208586.
34 X. Zeng, K. Xie, S. Liu, S. Zhang, J. Hao, J. Liu, W. K. Pang, J. Liu, P. Rao, Q. Wang, J. Mao, Z. Guo, *Energy Environ. Sci.*, 2021, **14**, 5947-5957.
35 F. Yang, J. A. Yuwono, J. Hao, J. Long, L. Yuan, Y. Wang, S. Liu, Y. Fan, S. Zhao, K. Davey, Z. Guo, *Adv. Mater.*, 2022, **34**, 2206754.
36 C. Liu, W. B. Jiang, D. Xie, W. Y. Diao, F. Y. Tao, X. Z. Wang, H. Z. Sun, W. L. Li, X. L. Wu, J. P. Zhang, *Small*, 2023, **19**, 2304751.
37 Z. Cao, X. Zhu, S. Gao, D. Xu, Z. Wang, Z. Ye, L. Wang, B. Chen, L. Li,

M. Ye, J. Shen, *Small*, 2021, **18**, 2103345.
38 P. Sun, L. Ma, W. Zhou, M. Qiu, Z. Wang, D. Chao, W. Mai, *Angew. Chem. Int. Ed.*, 2021, **60**, 18247-18255.
39 Q. Meng, R. Zhao, P. Cao, Q. Bai, J. Tang, G. Liu, X. Zhou, J. Yang, *Chem. Eng. J.*, 2022, **447**, 137471.
40 Y. Liu, J. Wang, J. Sun, F. Xiong, Q. Liu, Y. An, L. Shen, J. Wang, Q. An, L. Mai, *J. Mater. Chem. A*, 2022, **10**, 25029-25038.
41 J. Chen, N. Liu, W. Dong, Y. Xu, Y. Cao, S. Zhang, J. Hou, H. Bi, T. Lin, F. Q. Huang, *Adv. Funct. Mater.*, 2024, **34**, 2313925.
42 T. Zhou, Y. Mu, L. Chen, D. Li, W. Liu, C. Yang, S. Zhang, Q. Wang, P. Jiang, G. Ge, H. Zhou, *Energy Storage Mater.*, 2022, **45**, 777-785.
43 Z. Liang, C. Li, D. Zuo, L. Zeng, T. Ling, J. Han, J. Wan, *Energy Storage Mater.*, 2023, **63**, 102980.
44 H. Dou, X. Wu, M. Xu, R. Feng, Q. Ma, D. Luo, K. Zong, X. Wang, Z. Chen, *Angew. Chem. Int. Ed.*, 2024, **63**, e202401974.
45 C. Ma, X. Wang, W. Lu, K. Yang, N. Chen, H. Jiang, C. Wang, H. Yue, D. Zhang, F. Du, *Nano Lett.*, 2024, **24**, 4020-4028.
46 Y. Yang, Y. Li, Q. Zhu, B. Xu, *Adv. Funct. Mater.*, 2024, 2316371.
47 S. You, Q. Deng, Z. Wang, Y. Chu, Y. Xu, J. Lu, C. Yang, *Adv. Mater.*, 2024, **36**, 2402245.
48 Z. Yang, Y. Sun, S. Deng, H. Tong, M. Wu, X. Nie, Y. Su, G. He, Y. Zhang, J. Li, G. Chai, *Energy Environ. Sci.*, 2024, **17**, 3443-3453.
49 H. Lyu, S. Zhao, C. Liao, G. Li, J. Zhi, F. Huang, *Adv. Mater.*, 2024, 2400976.
50 S. Zhou, X. Meng, Y. Chen, J. Li, S. Lin, C. Han, X. Ji, Z. Chang, A. Pan, *Angew. Chem. Int. Ed.*, 2024, **63**, e202403050.
51 L. Hong, J. Guan, Y. Tan, Y. Chen, Y.-S. Liu, W. Huang, C. Yu, Y. Zhou, J.-S. Chen, K.-X. Wang, *Energy Environ. Sci.*, 2024, **17**, 3157-3167.